

NASA/TM-2011-217308



Design, Optimization, and Evaluation of Integrally-Stiffened Al-2139 Panel with Curved Stiffeners

David Havens

Lockheed Martin Aeronautics Company, Marietta, Georgia

Sandeep Shiyekar

Virginia Polytechnic Institute and State University, Blacksburg, Virginia

Ashley Norris

Lockheed Martin Aeronautics Company, Marietta, Georgia

R. Keith Bird

Langley Research Center, Hampton, Virginia

Rakesh K. Kapania

Virginia Polytechnic Institute and State University, Blacksburg, Virginia

Robert Olliffe

Lockheed Martin Aeronautics Company, Marietta, Georgia

November 2011

NASA STI Program . . . in Profile

Since its founding, NASA has been dedicated to the advancement of aeronautics and space science. The NASA scientific and technical information (STI) program plays a key part in helping NASA maintain this important role.

The NASA STI program operates under the auspices of the Agency Chief Information Officer. It collects, organizes, provides for archiving, and disseminates NASA's STI. The NASA STI program provides access to the NASA Aeronautics and Space Database and its public interface, the NASA Technical Report Server, thus providing one of the largest collections of aeronautical and space science STI in the world. Results are published in both non-NASA channels and by NASA in the NASA STI Report Series, which includes the following report types:

- **TECHNICAL PUBLICATION.** Reports of completed research or a major significant phase of research that present the results of NASA programs and include extensive data or theoretical analysis. Includes compilations of significant scientific and technical data and information deemed to be of continuing reference value. NASA counterpart of peer-reviewed formal professional papers, but having less stringent limitations on manuscript length and extent of graphic presentations.
- **TECHNICAL MEMORANDUM.** Scientific and technical findings that are preliminary or of specialized interest, e.g., quick release reports, working papers, and bibliographies that contain minimal annotation. Does not contain extensive analysis.
- **CONTRACTOR REPORT.** Scientific and technical findings by NASA-sponsored contractors and grantees.
- **CONFERENCE PUBLICATION.** Collected papers from scientific and technical conferences, symposia, seminars, or other meetings sponsored or co-sponsored by NASA.
- **SPECIAL PUBLICATION.** Scientific, technical, or historical information from NASA programs, projects, and missions, often concerned with subjects having substantial public interest.
- **TECHNICAL TRANSLATION.** English-language translations of foreign scientific and technical material pertinent to NASA's mission.

Specialized services also include creating custom thesauri, building customized databases, and organizing and publishing research results.

For more information about the NASA STI program, see the following:

- Access the NASA STI program home page at <http://www.sti.nasa.gov>
- E-mail your question via the Internet to help@sti.nasa.gov
- Fax your question to the NASA STI Help Desk at 443-757-5803
- Phone the NASA STI Help Desk at 443-757-5802
- Write to:
NASA STI Help Desk
NASA Center for AeroSpace Information
7115 Standard Drive
Hanover, MD 21076-1320

NASA/TM-2011-217308



Design, Optimization, and Evaluation of Integrally-Stiffened Al-2139 Panel with Curved Stiffeners

David Havens

Lockheed Martin Aeronautics Company, Marietta, Georgia

Sandeep Shiyekar

Virginia Polytechnic Institute and State University, Blacksburg, Virginia

Ashley Norris

Lockheed Martin Aeronautics Company, Marietta, Georgia

R. Keith Bird

Langley Research Center, Hampton, Virginia

Rakesh K. Kapania

Virginia Polytechnic Institute and State University, Blacksburg, Virginia

Robert Olliffe

Lockheed Martin Aeronautics Company, Marietta, Georgia

National Aeronautics and
Space Administration

Langley Research Center
Hampton, Virginia 23681-2199

November 2011

Acknowledgments

The work presented here was funded under NASA Subsonic Fixed Wing Hybrid Body Technologies NRA (NASA NN L08AA02C) with Ms. Karen M. Brown Taminger as the API. We are thankful to Ms. Taminger for her suggestions. The authors would like to thank our partners in the NRA project, Mr. John Barnes and Dr. Steve Englestad, both of Lockheed Martin Aeronautics Company of Marietta, GA, for technical discussions. Tests were conducted at NASA Langley Research Center under the Subsonic Fixed Wing Project.

The use of trademarks or names of manufacturers in this report is for accurate reporting and does not constitute an official endorsement, either expressed or implied, of such products or manufacturers by the National Aeronautics and Space Administration.

Available from:

NASA Center for AeroSpace Information
7115 Standard Drive
Hanover, MD 21076-1320
443-757-5802

Abstract

A curvilinear stiffened panel was designed, manufactured, and tested in the Combined Load Test Fixture at NASA Langley Research Center. The panel is representative of a large wing engine pylon rib and was optimized for minimum mass subjected to three combined load cases. The optimization included constraints on web buckling, material yielding, crippling or local stiffener failure, and damage tolerance using a new analysis tool named EBF3PanelOpt. Testing was performed for the critical combined compression-shear loading configuration. The panel was loaded beyond initial buckling, and strains and out-of-plane displacements were extracted from a total of 20 strain gages and 6 linear variable displacement transducers. The VIC-3D system was utilized to obtain full field displacements/strains in the stiffened side of the panel. The experimental data were compared with the strains and out-of-plane deflections from a high fidelity nonlinear finite element analysis. The experimental data were also compared with linear elastic finite element results of the panel/test-fixture assembly. Overall, the panel buckled very near to the predicted load in the web regions.

1 Introduction

A new analysis tool, *EBF3PanelOpt*, is being developed for design and optimization of complex multifunctional aircraft structural concepts. Application of this new analysis tool is towards pressurized non-circular fuselage structures within hybrid wing/body vehicles. In such vehicles, complex structural load cases are not well characterized using current design databases. *EBF3PanelOpt* can be used to integrate materials and structural concepts to exploit emerging additive manufacturing processes. These processes offer the ability to efficiently fabricate complex structural configurations. The ultimate goal is to enhance aircraft performance and environmental responsibility through reductions in weight, emissions, and cabin noise. A secondary goal is to integrate functions such as acoustic damping, adaptive active aerodynamic controls, and aeroelastically tailored structures.

Development of this tool is being conducted under a NASA Research Announcement (NRA) contract at Virginia Polytechnic Institute and State University with support and aircraft manufacturing expertise provided through a subcontract with Lockheed Martin Aeronautics Company. The work is complementary to Electron Beam Freeform Fabrication (EBF³), an additive manufacturing research activity at NASA Langley Research Center (LaRC).

This paper describes the initial phases of development of the *EBF3PanelOpt* tool. The tool was used to design and optimize a structural panel with curved stiffeners. It was desired to select a realistic aircraft structural panel with "horizontal" and two "vertical" stiffeners for redesign with curved stiffeners and with cut-outs to demonstrate damage tolerance capabilities. A wing-mounted engine pylon rib panel was selected. In the case of this panel, the optimization was based on minimum mass subjected to constraints on buckling load, yielding, crippling or local stiffener failure, and damage tolerance under a combination of compression and shear loads. This optimization effort was used to evaluate the capability of the tool to handle complex loading conditions. The optimized panel design was used to fabricate an integrally-machined test panel using aluminum alloy 2139-T8. The panel was tested in the NASA LaRC Combined Loads Test Fixture (CLTF) [1] under a combined compression-shear loading case. The test results were compared against linear Finite Element Analysis (FEA) of the test fixture/panel assembly through which *EBF3PanelOpt* obtains the optimization constraints and a conventional high fidelity nonlinear FEA. The test results and analyses were used to assess the strengths and weaknesses of the

EBF3PanelOpt tool for the next version of its development as a tool for structural panel design and optimization.

2 *EBF3PanelOpt* Framework

A framework has been developed by researchers at Virginia Polytechnic Institute and State University for design optimization of curvilinear stiffened panels under in-plane and transverse loading [2-5]. The framework named *EBF3PanelOpt* is an object-oriented script written in PYTHON that interfaces with ABAQUS to perform finite element analysis on a panel with curvilinear, blade-type stiffeners and returns the mass of the panel and constraints on yielding, buckling, and crippling or local failure of the panel.

The *EBF3PanelOpt* script obtains design data from an optimizing software such as VisualDoc and translates the design data into ABAQUS. A schematic of the *EBF3PanelOpt* Framework may be seen in figure 1. After completion of the FEA, the script reads the results from the output file (*.odv) and calculates the responses. The responses include mass, buckling constraint, von Mises stress constraint, local crippling constraint, and damage tolerance constraint. The buckling constraint is calculated by:

$$\frac{1}{\lambda_0} \leq 1 \quad (1)$$

where, λ_0 is the buckling eigenvalue. The von Mises stress constraint is calculated by:

$$\frac{\sigma_{vm}}{\sigma_y} \leq 1 \quad (2)$$

where, σ_{vm} is the von Mises stress and σ_y is the material yield strength. The von Mises stress constraint is imposed using Kreisselmeier-Steinhauser criteria for constraint aggregation as described in [2]. The crippling constraint is calculated by:

$$\frac{|\sigma_{stiff}|}{F_{cc}} \leq 1 \quad (3)$$

where, σ_{stiff} is taken as the minimum principal stress in the stiffener and F_{cc} is the maximum allowable stress in the stiffener given by:

$$F_{cc} = \begin{cases} \sigma_y, & 0.61525 \left(\frac{b\sqrt{\sigma_y/E}}{t} \right)^{-0.78387} > 1 \\ 0.61525 \sigma_y \left(\frac{b\sqrt{\sigma_y/E}}{t} \right)^{-0.78387}, & 0.61525 \left(\frac{b\sqrt{\sigma_y/E}}{t} \right)^{-0.78387} \leq 1 \end{cases} \quad (4)$$

where, E is Young's modulus of the stiffener material, b is stiffener height, t is stiffener thickness. The maximum allowable stress formula, Eq. (4), is obtained from page 444 of [6].

The damage tolerance constraint is given by

$$K_{eff} \leq K_{IC} \quad (5)$$

where K_{IC} is the plane strain fracture toughness. The effective stress intensity factor K_{eff} is computed as:

$$K_{eff} = \sqrt{K_I^2 + \alpha K_{II}^2} \text{ where } 0 \leq \alpha \leq 1 \quad (6)$$

where K_I and K_{II} are Mode I and Mode II stress intensity factor, respectively.

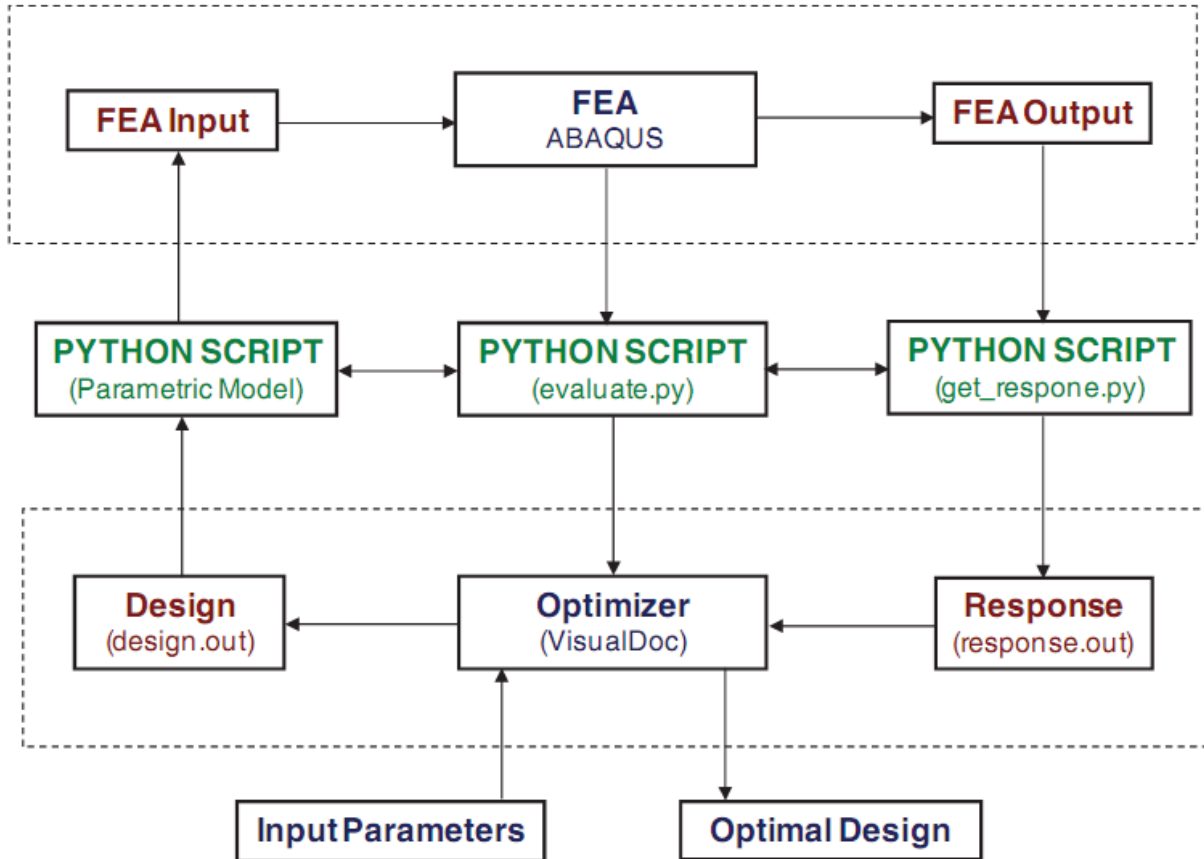


Figure 1. Schematic of *EBF3PanelOpt* Framework.

2.1 Parametric Modeling of the Panel

The design optimization problem of the complex configuration in this study used a baseline configuration consisting of a rectangular stiffened panel with two or four curvilinear stiffeners and one or two circular cutouts. The loading, material properties, and design constraints for the baseline panel configuration were provided by Lockheed Martin Aeronautics Company (Lockheed Martin) as representative of typical aircraft structure for this design optimization study. Except where noted, the material used in the design examples for FEA was Al 2139-T8. The optimization was performed using two or four blade-type curvilinear stiffeners. Shape design variables such as stiffener orientations and curvatures and sizing design variables such as stiffener and web dimensions and panel thickness were used. Due to the current capability of CAE in ABAQUS, which is limited to creating curved lines by creating y splines throughout nodal points only, it is very difficult to handle the issue of the curve going over the domain of the plate.

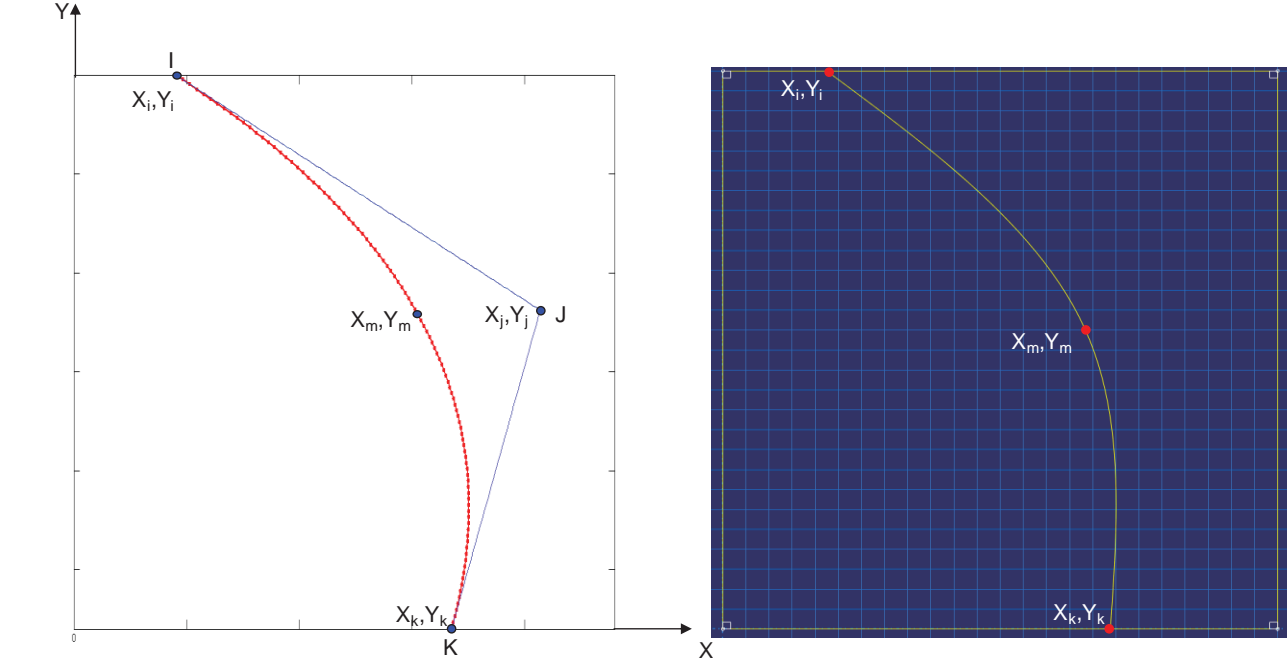
Except for the end points of the curve that are on the boundary of the domain, it is in generally difficult to know whether or not the curve intersects the boundary of the domain in the optimization problem.

An “approximate” method was used to overcome the problem in the optimization problem by creating curved lines using control points. The Bezier curve-based technique using three control points was used in the optimization problem (see figure 2). The Bezier curve equation is in the parametric form as:

$$\begin{Bmatrix} x \\ y \end{Bmatrix} = (1-t)^2 \begin{Bmatrix} x_i \\ y_i \end{Bmatrix} + 2t(1-t) \begin{Bmatrix} x_j \\ y_j \end{Bmatrix} + t^2 \begin{Bmatrix} x_k \\ y_k \end{Bmatrix} \tag{7}$$

where $t \in [0,1]$, and $(x_i, y_i), (x_j, y_j), (x_k, y_k)$ are coordinates of the control points $I, J,$ and $K,$ respectively.

To create a curved line in ABAQUS using the spline technique passing through points, one more point (x_m, y_m) was interpolated from the Bezier curve at $t=0.5$ as shown in figure 2, after which a spline curve through three points $(x_i, y_i), (x_m, y_m), (x_k, y_k)$ can be created. This spline curve is slightly different from the Bezier curve as described, and in some cases, it still intersects the boundary of the domain, although three control points lie in the domain of the plate. This method is considered "approximate" because several trials are needed to determine the suitable range of these control points. There are 6 design variables needed to define the curvilinear stiffeners using this technique. These design variables are used to obtain optimal stiffener orientation and curvature, while the sizing design variables present the heights and thickness of stiffeners, and thickness of the panel. Tolerances on design variables are used while specifying lower and upper bounds on these design variables in order to avoid problems in geometry creation.



a) Create a Bezier Curve using Three Control Points b) Create a Spline throughout Three Points in ABAQUS

Figure 2. Method to Create a Curvilinear Stiffener in ABAQUS

A parametric model was created using Macro Manager in ABAQUS to record the PYTHON script of the parametric model. The design variables as described above were labeled in the PYTHON script. This script was called `stiffened_plate.py.template`, which plays the most important role in the program. The function of the “`stiffened_plate.py.template`” script was to carry out analysis to have outputs on buckling, damage tolerance, and stress (see figure 1) for evaluating the responses and send them to the optimizer.

3 Combined Loads Test Fixture

The Combined Loads Test Fixture (CLTF) was developed by researchers at the NASA Langley Research Center (LaRC) to perform combined compression-shear load tests on 24-inch x 28-inch panels [1]. A detailed description of the design, assembly, and operation of the test fixture can be found in [1]. Figure 3 shows the test system without the panel installed. The upper L-shaped shear fixture is bolted to the upper compression platen of a 300-kip capacity screw-driven compression test system. The bottom of the lower shear fixture rests on roller guides affixed to the lower platen to allow lateral motion. The upright edge of the lower shear fixture is attached to a hydraulic ram to apply the shear loads. A steel picture frame-type support is attached to the test specimen via a double row of fasteners (see figure 4). The picture frame edges are pinned together at the corners to allow in-plane rotation. This support provides the clamped boundary condition to the aluminum tabs while allowing the panel to deform to a parallelogram shape. After installation of the test panel the CLTF, shear load bars (not shown in figure 3) are attached across the upper and lower shear frames to provide for a self-reacting shear load mechanism.



Figure 3. Compression-Shear Test System without Test Panel Installed.



Figure 4. Picture Frame Support Mounted on a Generic Test Panel.

4 Panel Design and Optimization

A 24-inch x 28 inch curvilinear stiffened panel was designed using *EBF3PanelOpt* software and VisualDoc optimization tool. The particle swarm optimization (PSO) [7] was used to estimate the global minimum mass satisfying constraints on buckling, crippling and yielding. Detailed optimized design of panel is presented in section 4.3.

4.1 Test Fixture Interface

Early study of the CLTF indicated that it only transmitted a portion of the compression load into the panel while 100% of the shear load was transmitted to the panel [2]. Therefore, to facilitate the loading and boundary conditions as closely as possible to those imposed by the CLTF, a reduced grid-point interaction model of the test fixture/panel interface is utilized within the *EBF3PanelOpt* framework to apply the loading and boundary conditions during optimization. The reduced model via a superelement was developed from a detailed nonlinear finite element model of the fixture developed by Lockheed Martin, illustrated in figure 5.

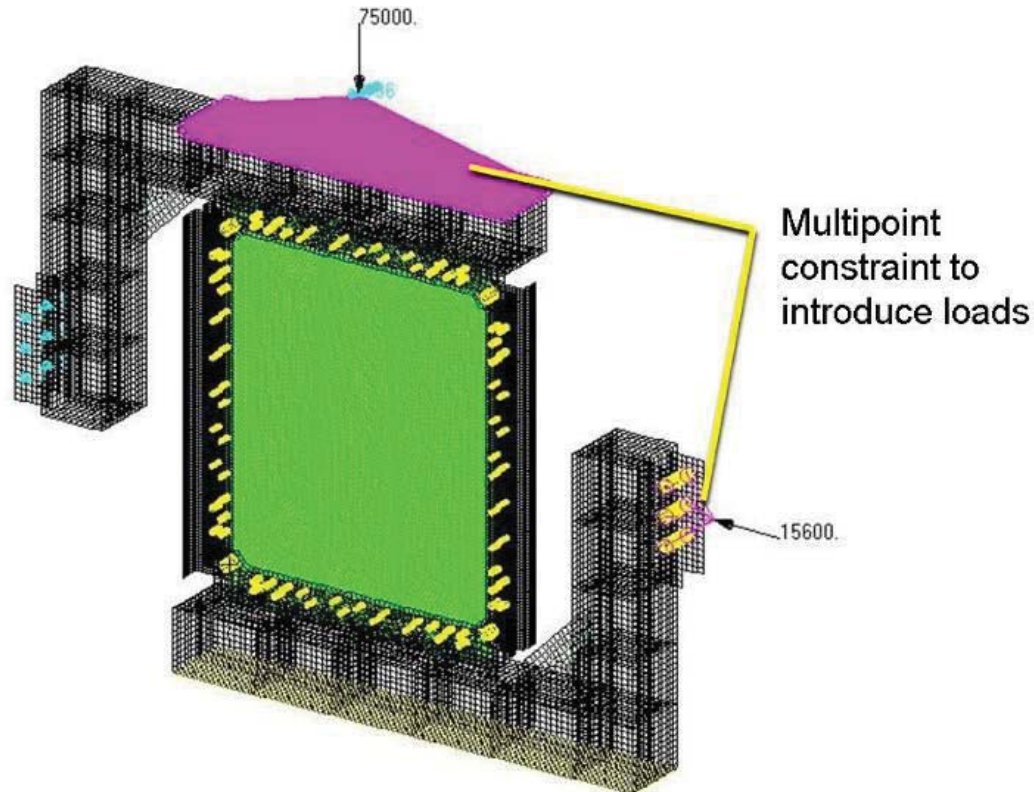


Figure 5. Nonlinear Finite Element Model of Test Fixture/Curvilinear Stiffened Panel Assembly.

4.2 Nonlinear Finite Element Model

A nonlinear finite element model (FEM) of the CLTF was developed by Lockheed Martin Aeronautics Company. The FEM includes both elastic-plastic (for the aluminum) and geometric nonlinearity and thus is suitable for the post-buckling analysis. The test fixture FEM was developed to interface to a panel model generated by the *EBF3PanelOpt*. The test fixture was modeled using a total of 44,186 shell, beam, and gap elements. Shell elements were used to model the steel test fixture upper and lower L-arms of the CLTF as well as the picture frame support secured to the panel (see figure 6). The test fixture is constructed predominately from 15-5 (or 17-4) H1025 stainless steel [1]. The material properties used for the test fixture FEM are given in table 1. A linear stress-strain relation was used for the test fixture as the fixture's thickness precludes significant material nonlinearity therein.

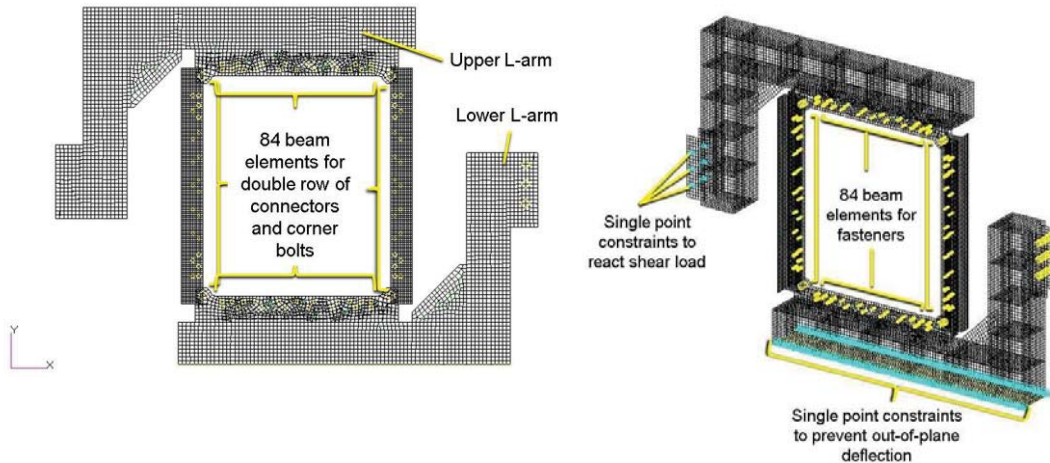


Figure 6. Steel Shell Elements in the Nonlinear Test Fixture Model and the Single Point Constraints Applied to the Test Fixture Model.

The compressive load is introduced into a single node above the upper L-arm and applied to the upper L-arm using a multipoint constraint. The shear load is introduced in a similar manner to the lower L-arm. In each case, two concentric nodes attached by zero length spring elements were used to provide the appropriate stiffness to the load introduction location. The stiffnesses of these springs were chosen by correlating data from previous Lockheed Martin tests in the CLTF.

Gap elements were used in the FEM to numerically model the “rollers” on which the lower L-arm sits. The gap elements allow the test fixture to pull off the rollers while providing a very large stiffness to prevent penetration. The bottom of the test fixture was constrained to prevent out-of-plane deflection using two parallel rows of single point constraints applied to the exterior nodes on both sides of the lower L-arm. The shear load was reacted using single point constraints applied to the bolt locations on the top L-arm (see figure 6).

The aluminum test panel was modeled using shell elements. The test panel FEM was provided by the *EBF3PanelOpt* analysis software and modified to include the elastic-plastic material model. Initial eccentricity of the panel was provided moving the nodes to match the shape of the first buckling mode, scaled to a peak amplitude of 0.0001inch, thus producing a slightly imperfect panel to help guide the geometric nonlinear analysis off the trivial solution path. The adhesively bonded steel tabs were modeled using shell elements with an elastic-plastic material law. Zero-length spring elements with stiffness of 41,250 lb/inch were used to model the adhesive bond. The FEM of the test panel assembly can be seen in figure 7.

The double row of fasteners, the four corner fasteners, and the bolts through which the shear load was introduced were modeled using beam elements with appropriate material and geometric properties assigned. The fasteners, highlighted in yellow, are shown figure 6.

Table 1. Material Properties used in the Nonlinear Finite Element Model.

| | 15-5 (or 17-4) H1025 Stainless Steel | Al 2139-T8 |
|----------------------------|--------------------------------------|------------|
| Young's Modulus, E [ksi] | 29,200 | 10,600 |
| Poisson's ratio, ν | 0.32 | 0.33 |
| Yield Stress, [ksi] | 152.9 | 68.1 |

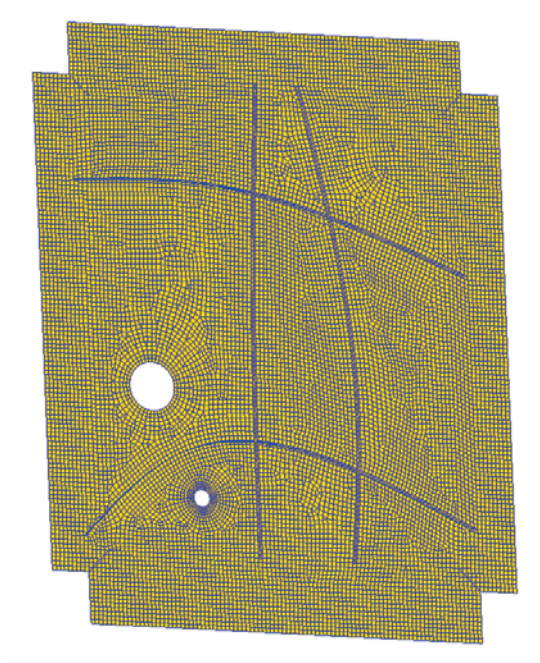


Figure 7. Finite Element Model of test panel.

4.3 Optimization of Two and Four Curvilinear Stiffeners

A baseline panel design from Lockheed Martin (shown in figure 8) was used to perform the optimization with multi-constraints imposed on buckling, damage tolerance, vonMises stress, and crippling under two load cases (see figure 9). Two curvilinear stiffeners were used for the optimized design and were created by the “approximate” Bezier curve using three control points as described above. The design variable scheme is shown in figure 10. The baseline is a clamped edge, complex panel with two cutouts. Load case (a) presents the panel under maximum compression load and load case (b) presents the panel under maximum tension load. The panel was designed with two rings around two cutouts and with two or four curvilinear stiffeners.

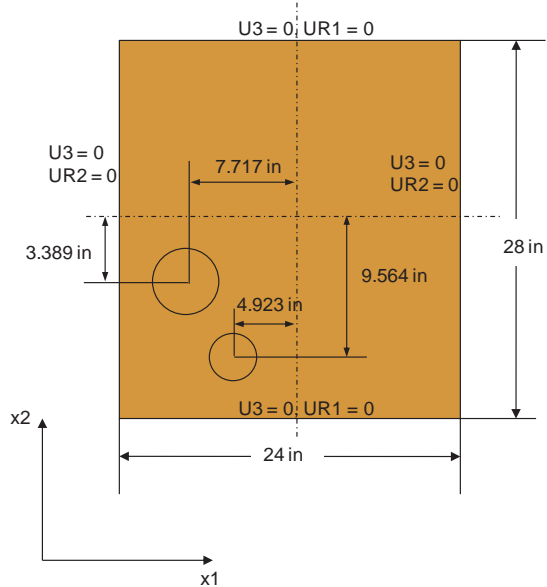


Figure 8. Lockheed Martin Baseline.

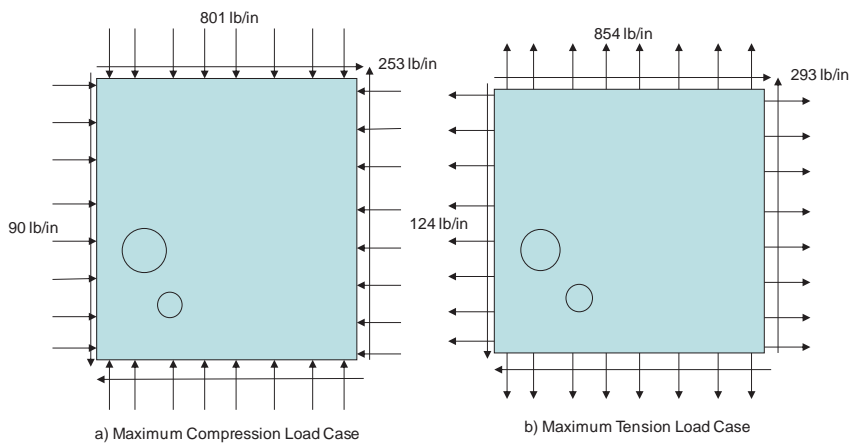


Figure 9. Scheme for Multi-Load Cases.

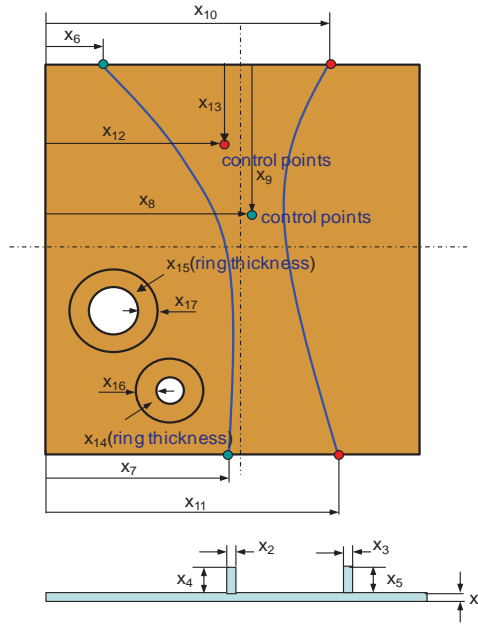


Figure 10. Design Variables for Optimization Problem with Two Curvilinear Stiffeners.

The optimization results of the Lockheed Martin baseline using two curvilinear stiffeners with multi-constraints under two load cases are summarized in table 2. The constraints on buckling and on crippling are active and become critical while the constraints on vonMises stress and damage tolerance in this problem are not critical. This conclusion confirmed the investigation on the fracture, stress and buckling analysis of the baseline for doing the optimization problem. Therefore, to save computation, the inactive constraints were checked after the optimization for the optimal configuration. In this case, the damage tolerance constraint was 0.0806 while the damage tolerance criterion for the stress concentrations around cutouts was also satisfied, with the damage tolerant constraint being 0.7436.

Table 2. Optimization results for Lockheed Martin Cutout-panel with Multi-Constraints under Multi-Load Cases: In the Case of Two Curvilinear Stiffeners.

| | Optimal Design Parameters | Constraint on Crippling | Constraint on Von-Mises Stress | Constraint on Buckling |
|-------------------------------|---------------------------|-------------------------|--------------------------------|------------------------|
| Mass | 7.27838 lb (3.3014 kg) | 0.80694 | 0.3606 | 0.9990 |
| Skin Thickness | 0.1018 in (2.5867 mm) | | | |
| Ring Thickness for Small Hole | 0.2957 in (7.5096 mm) | | | |
| Width of Ring for Small Hole | 0.8176 in (20.7678 mm) | | | |
| Ring Thickness for Big Hole | 0.1672 in (4.2470 mm) | | | |
| Width of Ring for Big Hole | 1.3669 in (34.7191 mm) | | | |
| Height of Stiffener 1 | 1.1473 in (29.1408 mm) | | | |
| Thickness of Stiffener 1 | 0.0639 in (1.6234 mm) | | | |
| Height of Stiffener 2 | 1.5059 in (38.2492 mm) | | | |
| Thickness of Stiffener 2 | 0.0630 in (1.6003 mm) | | | |

Table 3. Optimal Design Variables for Lockheed Martin Cutout-panel with Multi-Constraints under Multi-Load Cases: Case of Two Curvilinear Stiffeners.

| Design Variable | Meaning | Low Bound (in) | Upper Bound (in) | Optimal Design (in) |
|------------------------|-------------------------------|-----------------------|-------------------------|----------------------------|
| X1 | Skin thickness | 0.063 | 0.177 | 0.1018 |
| X2 | Stiffener thickness 1 | 0.063 | 0.315 | 0.0639 |
| X3 | Stiffener thickness 2 | 0.063 | 0.315 | 0.0630 |
| X4 | Stiffener height 1 | 0.394 | 1.97 | 1.1473 |
| X5 | Stiffener height 2 | 0.394 | 1.97 | 1.5059 |
| X6 | Control point end | 0.27 | 11.5 | 5.4368 |
| X7 | Control point end | 9.7 | 11.5 | 10.7631 |
| X8 | Control point mid | 9.7 | 11.5 | 9.7533 |
| X9 | Control point mid | 0.27 | 14 | 13.3645 |
| X10 | Control point end | 12 | 23.2 | 12.5000 |
| X11 | Control point end | 12 | 23.2 | 16.7639 |
| X12 | Control point mid | 12 | 23.2 | 19.7008 |
| X13 | Control point mid | 0.27 | 27.73 | 24.8921 |
| X14 | Ring thickness for small hole | 0.063 | 0.315 | 0.2957 |
| X15 | Ring thickness for big hole | 0.063 | 0.315 | 0.1672 |
| X16 | Ring width for small hole | 0.4 | 1.6 | 0.8176 |
| X17 | Ring width for big hole | 0.4 | 1.6 | 1.3669 |

Table 3 shows the optimal parameters for all 17 design variables. The optimal design configuration is shown in figure 11 and the first four buckling mode shapes are shown in figure 12. The eigenvalues of the first four buckling modes of the optimal design configuration are very similar. During the panel optimization process, the eigenvalues of the first nine buckling modes were extracted and analyzed. The optimization was carried out using the Particle Swarm Optimization (PSO) with 40 particles after 69 iterations (see figure 13). The 69-iteration PSO result was used as the starting point for the Gradient-Based Optimization (GBO). The converged results of the GBO were obtained after 7 iterations and are shown in figure 14.

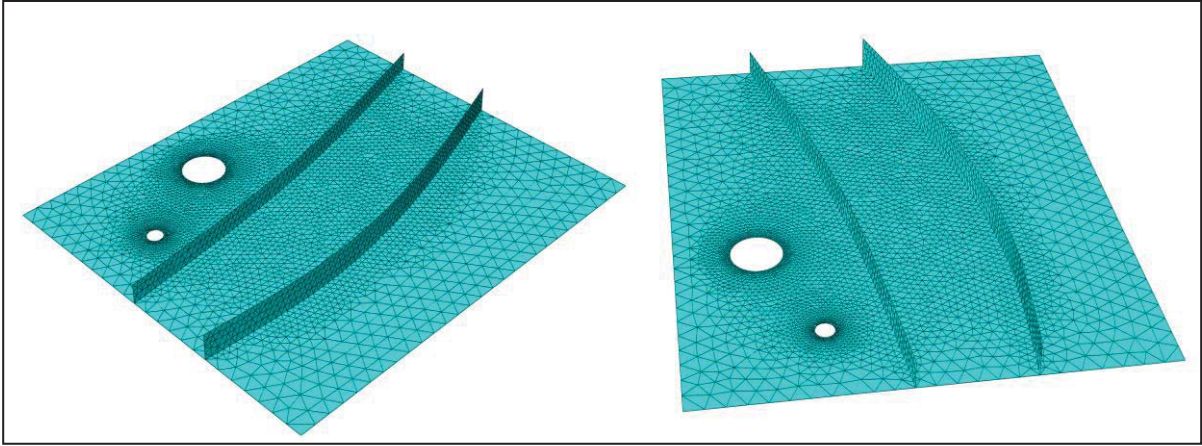


Figure 11. Optimal Design Configuration for Lockheed Martin Panel using PSO and Gradient Based Optimization: Case of Two Curvilinear Stiffeners

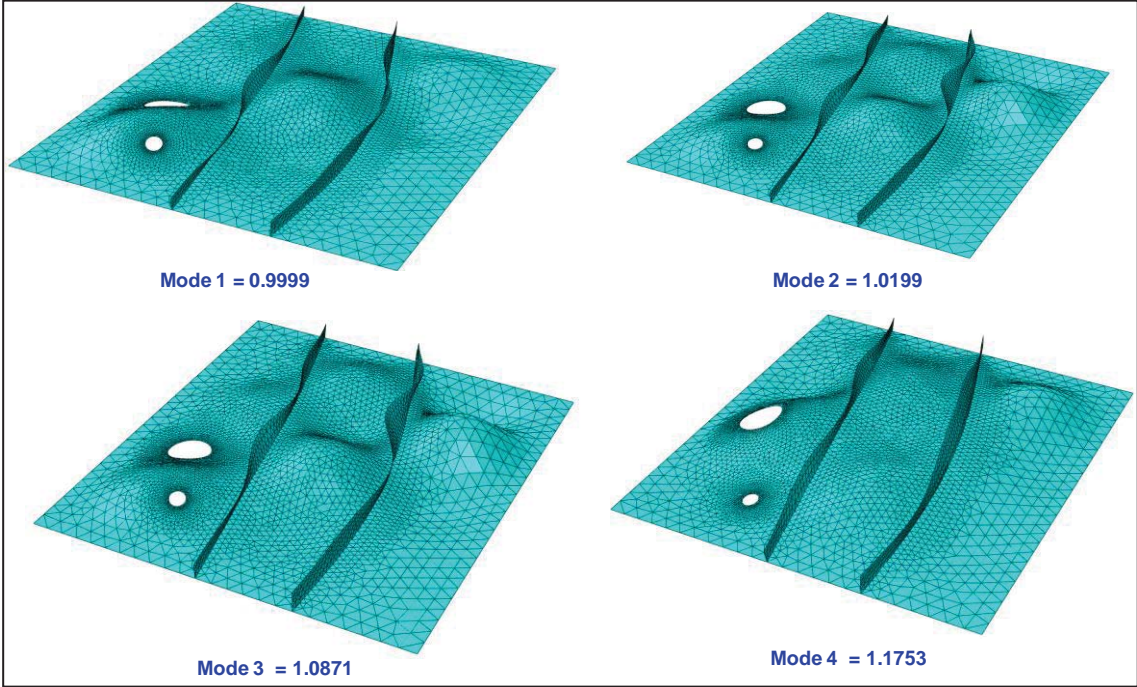


Figure 12. First Four Buckling Mode Shapes and eigenvalues for the Optimal Design Configuration using Two Curvilinear-Stiffeners.

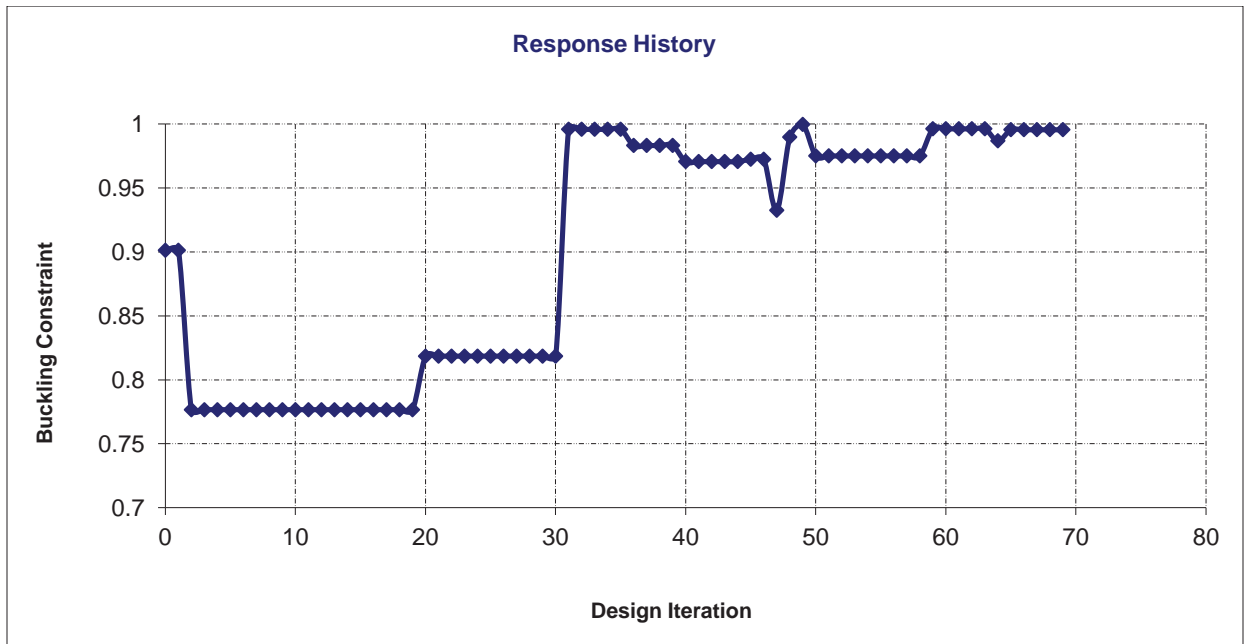
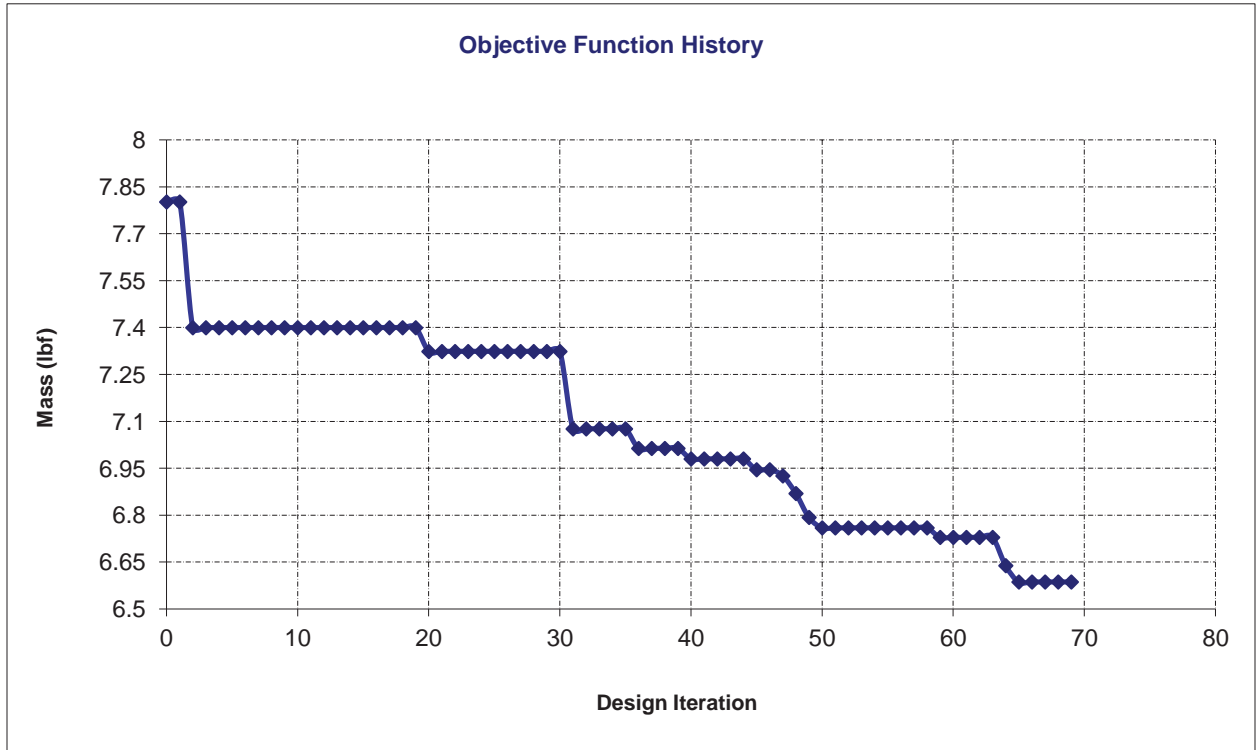


Figure 13. Optimization History for the Objective Function (Mass) and Buckling Constraint for Optimization of Lockheed Martin Panel using the PSO algorithm with 69 Iterations

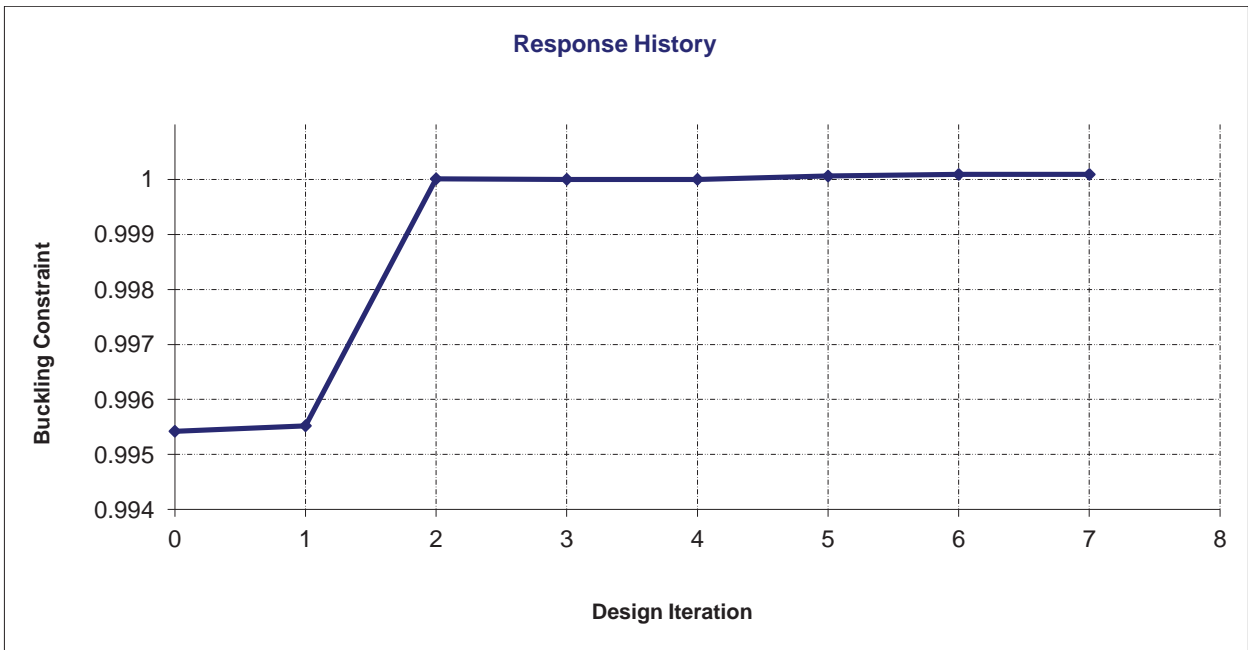
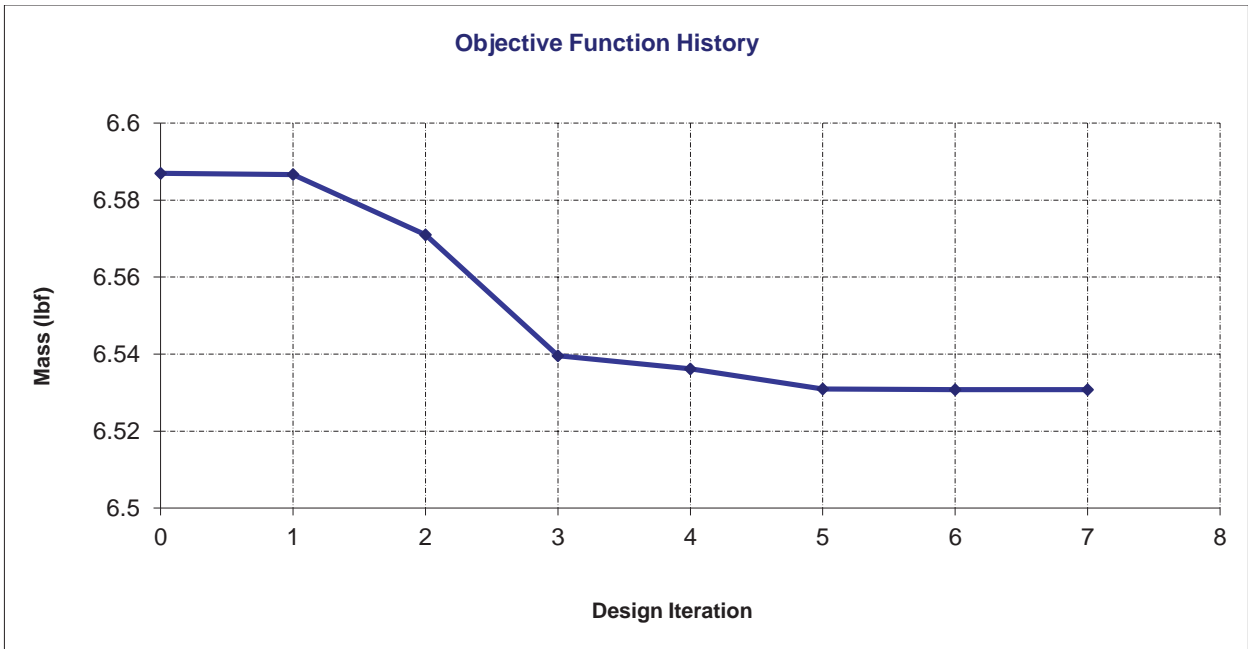


Figure 14. Optimization History for the Objective Function (Mass) and Buckling Constraint for Optimization of Lockheed Martin Panel using the GBO algorithm with 7 Iterations.

Innovative capabilities in the programming code were developed by VPI in version 2 of *EBF3PanelOpt*. The main objective was the design optimization of a curvilinear stiffened panel. Using the same simulation of loading, constraints and design criterion as per the two curvilinear stiffener cases, a four stiffener design was also optimized using the program. The resulting design was a panel with a weight of 6.820 lbf, which was 6.8 % less than the weight of the Lockheed Martin baseline with straight stiffeners. To validate these results of design optimization, Lockheed Martin generated experimental results for comparison. Figure 15 shows the panel with four curved stiffeners optimized using *EBF3PanelOpt* v2.0 with maximum von Mises stress and mode I eigenvalue contours.

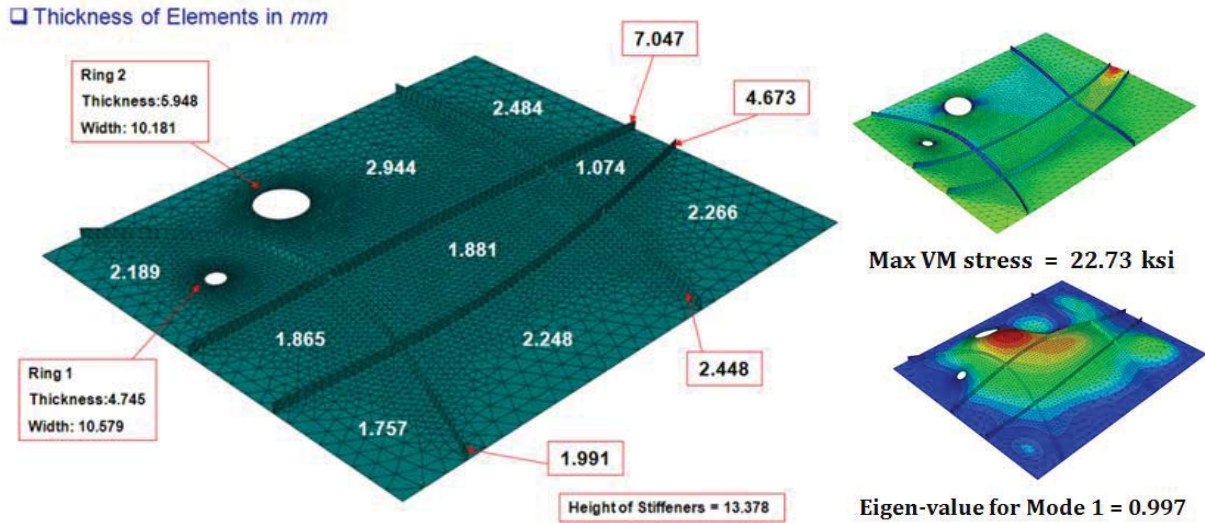


Figure 15. VT Optimized Panel using *EBF3PanelOpt* v2.0.

EBF3PanelOpt v2.0 predicted that the panel was buckling critical for the maximum compressive load case. A CATIA model of this panel was generated and used to manufacture the innovative panel design as shown in figure 16.

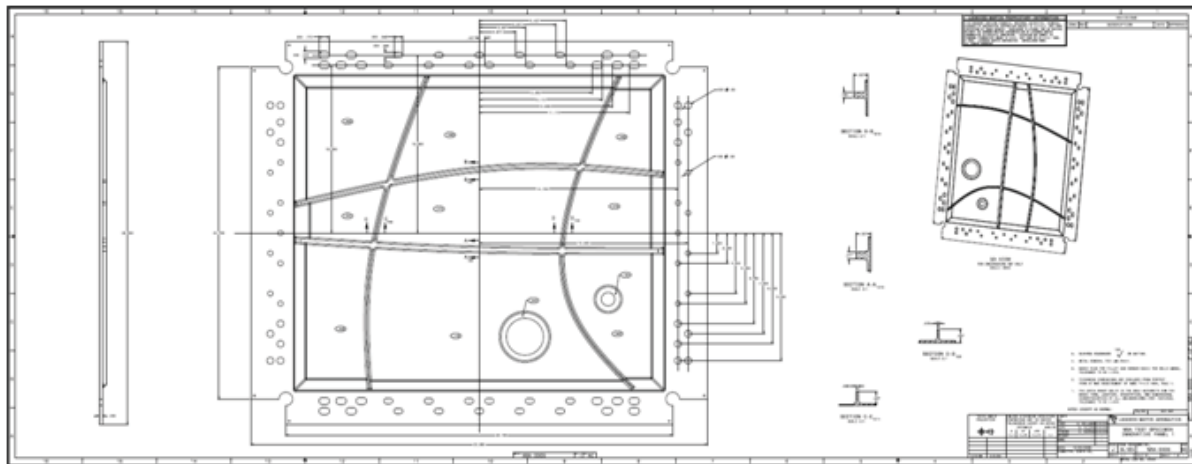


Figure 16. Panel Design for Manufacturing

5 Panel Manufacturing

A solid model of the curvilinear stiffened panel was converted to a detailed CAD file in CATIA V5 by Lockheed Martin. The geometry is included with fillets at the panel/stiffener intersections. The 24-inch x 28-inch panel was extended to include 2.94 inch x 24 inch tabs along the top and bottom edges with the bolt pattern specified by the CLTF (see figure 17). 2.25 inch x 28 inch tabs were also included along the left and right edge of the panel. While the panel had thickness of 0.104 inch, the tabs were required to be 0.25 inch to facilitate the interface between the CLTF and panel. A thickness taper was included to reduce the thickness from 0.25 inch to 0.104 inch. The geometry is included with stiffener run-outs at the ends.

The baseline optimized test article was then machined with blade stiffeners. This panel was machined from 2-inch thick aluminum alloy 2139-T8 plate stock and all required tolerances were met after the initial panel was determined to require some rework.

After the panel was machined and inspected, 4140 steel tabs conforming to the NASA combined loading fixture drawings [1] were adhesively bonded using Hysol EA9395 with 0.005-inch diameter glass micro-balloons added for bond-line control. These bonds were cured at room temperature for 24 hours then postcured at 200 °F to prevent any residual thermal expansion stresses at the bond-line. The panel was then crated and shipped to NASA LaRC for testing. The machined panel is shown in figure 17.

A surface profile of the test panel was generated using laser scanning techniques. Figure 18 shows the deviation of the laser-scanned surface from that of the original CAD file of the panel. The center region of the panel has surface profile of the original CAD file. However, the laser scan data indicate that the top and bottom ends of the panel are bowed approximately 0.1 inch towards the stiffener side of the panel.



Figure 17. Picture of the Al-2139 Test Panel without Steel Tabs.

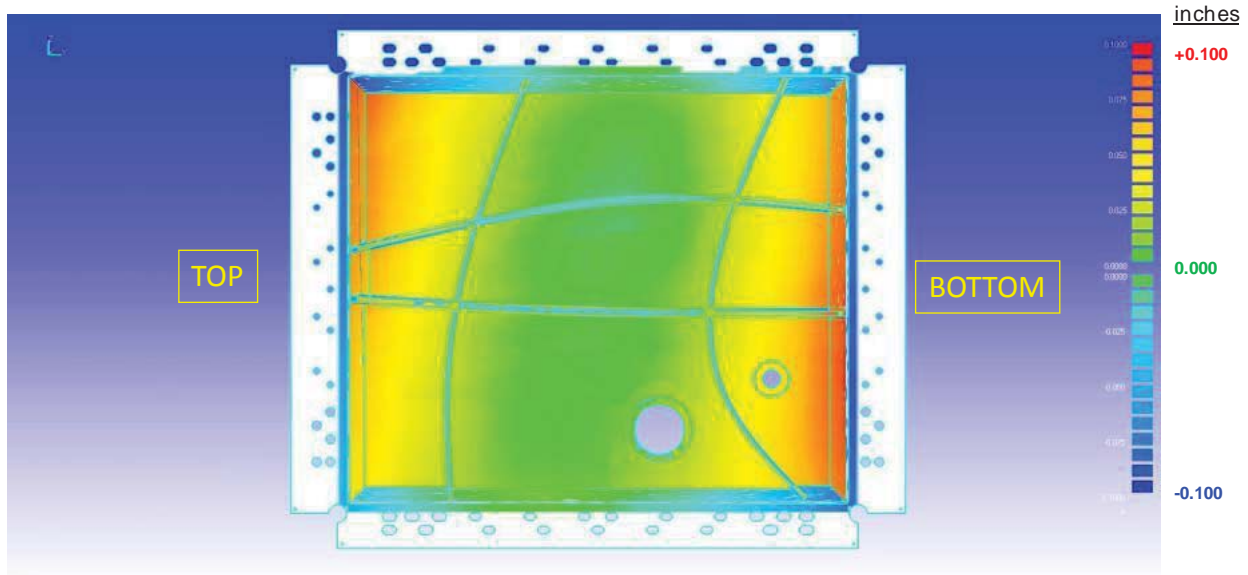


Figure 18. Out-of-plane distortion of fabricated test panel measured by scanning laser profilometer.

6 Combined Load Compression-Shear Test

A combined load compression-shear test was conducted at NASA LaRC on the panel using the CLTF. Linear variable displacement transducers (LVDTs) were attached to three corners of the top compression platen to measure panel end shortening and three LVDTs were attached to the shear fixture to measure shear displacement.

A total of 20 strain gages were attached to the skin of the panel. Ten of the gages were $0^\circ/45^\circ/90^\circ$ rosettes and 10 of the gages were uniaxial gages aligned parallel to the compression load direction. In addition, 6 more uniaxial gages were attached to selected stiffeners. A description of the strain gage locations is provided in appendix A. Both sides of the panel were spray-painted with a speckled pattern to facilitate strain and displacement measurements using a VIC-3D automated stereophotogrammetric technique. The panel was installed into the CLTF. The lateral shear load hydraulic ram was attached to the CLTF's lower shear frame. The LVDT support brackets and 6 LVDTs were installed into the test system and attached to the smooth side of the panel to measure out-of-plane displacement. A description of these LVDT locations is provided in appendix B.

The data acquisition system was configured to scan and record all of the instrumentation at a rate of 1 scan per second. The load, displacements, and select strain gages were monitored on a real-time display during the test. Two VIC-3D systems were configured to obtain full-field stereophotogrammetric displacement/strain measurements on the upper half and the lower half of stiffened side of panel. In addition to the VIC-3D cameras, video cameras were set up to record behavior of both the skin and stiffened sides of the panel during the test. Figure 19 shows the test system with the panel installed and ready for testing.

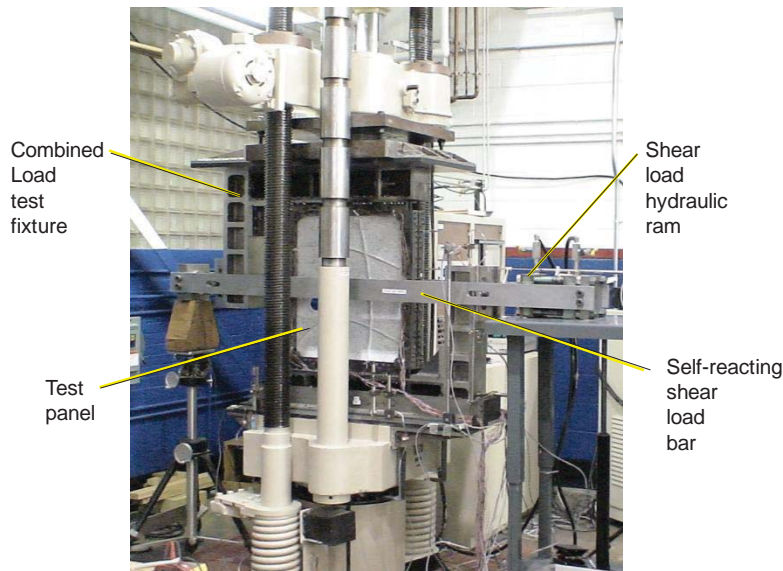


Figure 19. Compression-Shear Test System with Test Panels Installed.

The test system was configured to apply compression load and shear load simultaneously at a load ratio of 0.316 (shear load ÷ compression load). The compression load rate of 4,000 lbs/min was used. Two preliminary tests were conducted up to a maximum compression load of 5,000 lbs to ensure that the instrumentation was operational and that the load ratio was correct. The data acquisition and VIC-3D systems were started and load application was initiated. When the panel attained a compression load of 36,800 lbs and a shear load of 11,400 lbs a buckling event occurred and the compression load decreased rapidly by 600 lbs. The shear load controller was not able to adequately follow the compression load command signal and rapid oscillations in the shear actuator began. The test was stopped and the panel was unloaded. Once the load was removed, no apparent permanent panel deformation was observed.

The shear load controller tuning was adjusted and the compression-shear test was initiated again. Loading proceeded past the maximum load attained during the first test without event. Several loud "pops" were heard during loading. The panel attained a compression load of 54,600 lbs and a shear load of 16,800 lbs, at which point a very loud bang occurred. The shear load dropped to zero, but the compression load kept increasing and the test panel appeared to remain intact. The test was stopped and the panel was unloaded. It was discovered that the bolt connecting the shear load cell to the shear load frame had fractured, resulting in the loud noise and the loss of shear load. Inspection of the test system indicated that the shear load train hydraulic ram was operating in a direction opposite to the planned direction, thus applying a tensile load to the shear load cell bolt and resulting in bolt fracture. Removal of the panel from the test frame also revealed that three of the steel tabs had debonded from the edge of the panel. These debonds most likely were the source of the popping sounds during the test.

Post-test inspection of the panel showed a small permanently deformed area in the top center region near strain gage #A1. Figure 20 shows post-test photographs of the skin and stiffened sides of the test panel illustrating regions where the tabs debonded and the permanent buckled occurred. Figure 21 shows the extent of the buckled region. In the figure, one of the debonded steel tabs was placed on-edge across the buckled region to give a straight-edge reference for the amount of buckling. The skin buckled about 0.050 inch towards the stiffener side of the panel.

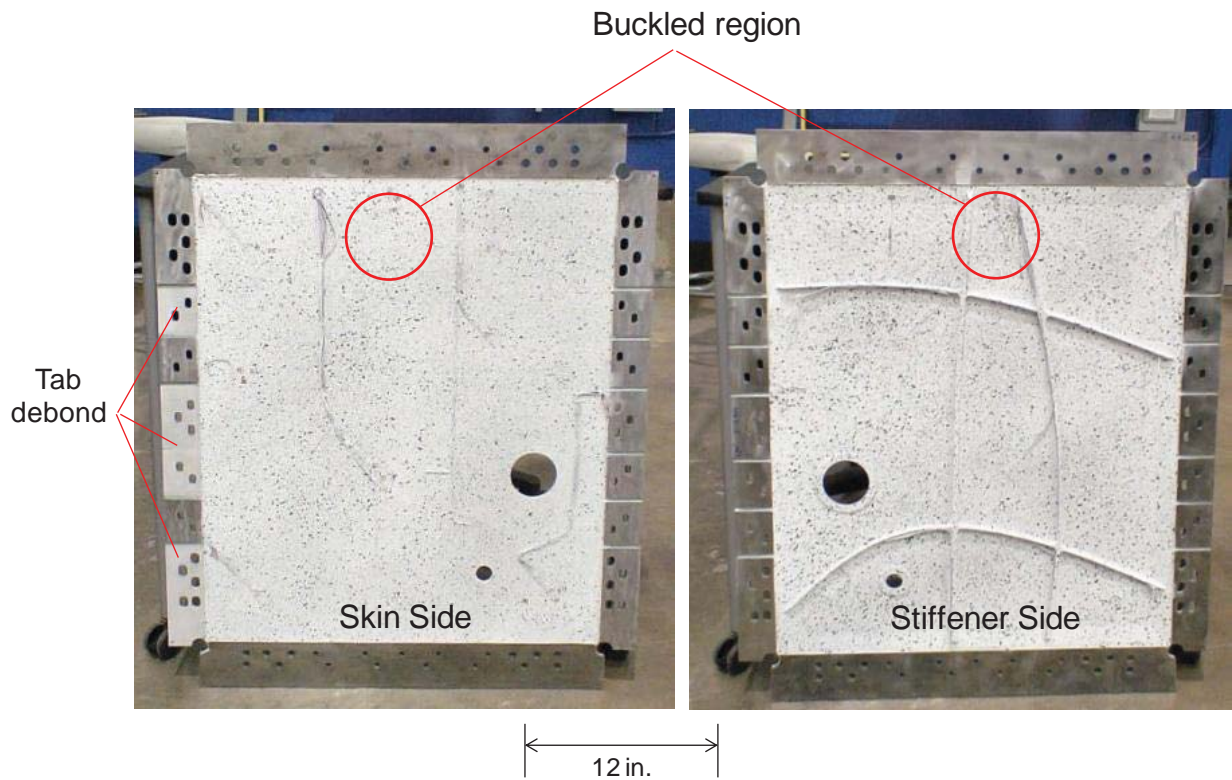


Figure 20. Post-Test Photograph of Test Panel with Debonded Tabs and Small Buckled Region.

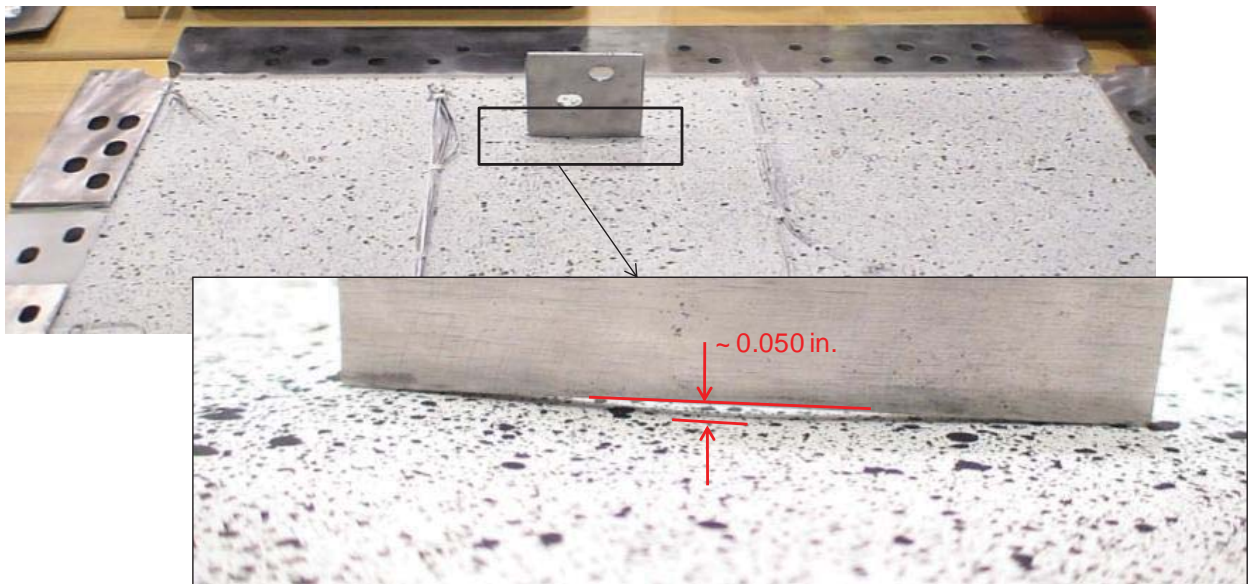


Figure 21. Post-Test Photograph of Test Panel showing Buckled Region.

7 Comparison of Results

Buckling

The first mode buckling test results are shown in Figure 22. This buckling occurs in the top center panel near strain gage A1. The solid blue line represents the predicted eigenvalue (or buckling load level) at a load factor of 0.77 which very closely matches our test data.

Normally, *EBF3PanelOpt* would not allow such a design to occur as it would violate the criteria for the panel to remain stable to limit load (an eigenvalue of 1.0). However, the panel design was optimized using a positive shear load (defined in Figure 9). The original analysis using a positive shear load predicted a buckling load factor level of 1.23 for the web at this panel location (i.e. this web should not buckle until 123% of limit load is achieved). However, as discussed previously, an anomaly in the test setup caused a negative shear load to be applied to the test panel. By reversing the shear load direction and using the same load magnitude, *EBF3PanelOpt* predicted a buckling load factor of 0.77 which matched the test results for an applied negative shear. This result that indicates that the direction of applied shear can have a significant effect on the design of curvilinear stiffened structure that is buckling critical. Based on this result, all of the predictions contained in this report are based on negative shear loading to allow a direct comparison to the test performed.

The test fixture also plays a role in comparing the *EBF3PanelOpt* results to the test results. As discussed in Section 4.3, the optimization used a clamped edge boundary condition with fully applied load. The test fixture (Section 4.1) only transmits a portion of the compression load into the panel, and has neither simple nor fully clamped edges. Using a FEM for predictions has minimized the discrepancy between the design and test data; however, some differences may still remain due to the nature of using a FEM representation.

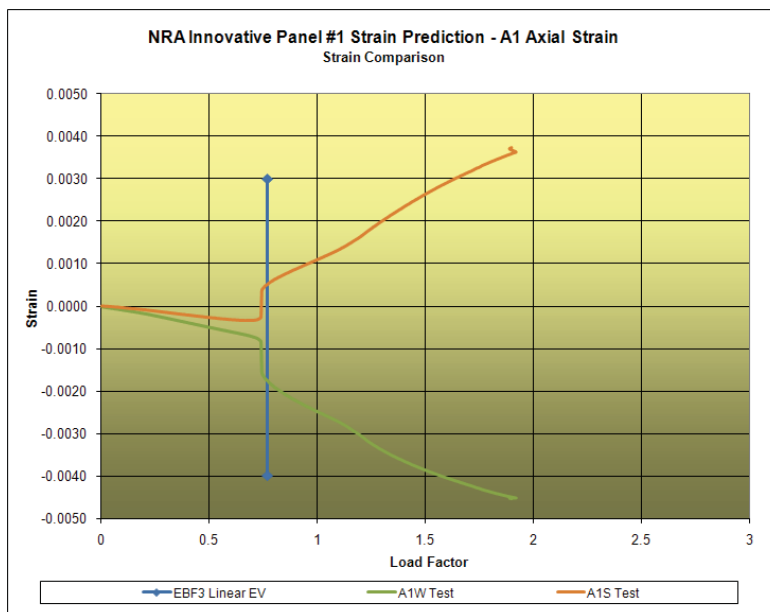


Figure 22. *EBF3PanelOpt* First Mode Buckling Prediction and Test Results. (Strain is presented in inch/inch.)

The next buckling mode test results are shown in Figure 23. The buckling is visible in the strain gage data for the upper and lower surface around a load factor of 0.93. The solid blue line shows the predicted eigenvalue at 0.93. This gage is near the center of the panel and represents the first “global” buckling mode (meaning multiple webs are affected by this mode shape).

Appendix C contains the data for all of the strain gages and the *EBF3PanelOpt* predictions for this test. Overall the panel buckled very near the predicted load factor level for each of the web regions. Based on the test results, the panel failed by buckling as predicted by the sizing mode and the buckling load compared well to that predicted by *EBF3PanelOpt*.

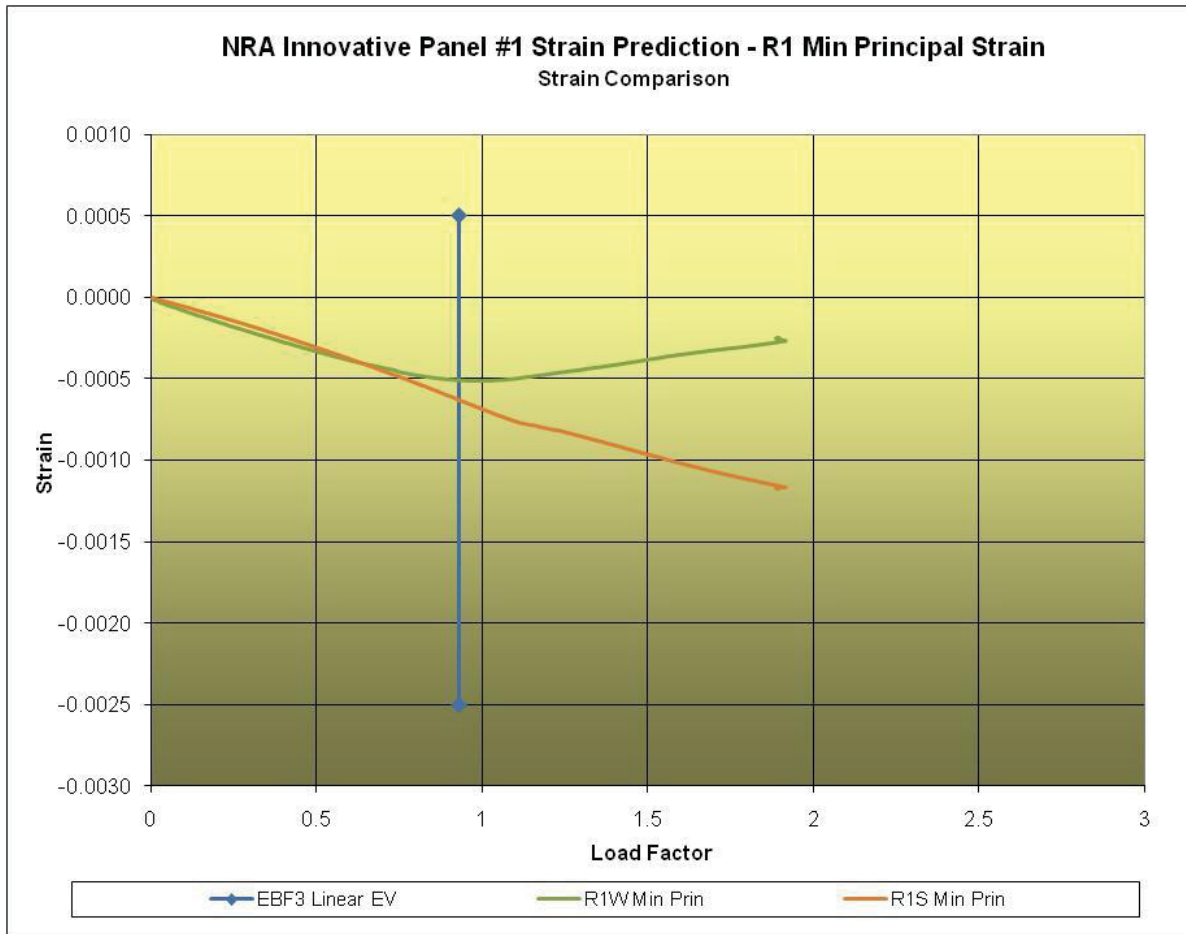


Figure 23. *EBF3PanelOpt* Second Mode Buckling Prediction and Test Results. (Strain is presented in inch/inch.)

Out-of-Plane Displacement

Six LVDT's were used during the test to monitor the out of plane displacement of the panel. All of the LVDT's were arranged on the flat side of the panel. Using the cutouts for positional reference, the locations are shown below in Figure 24 as D1 – D6.

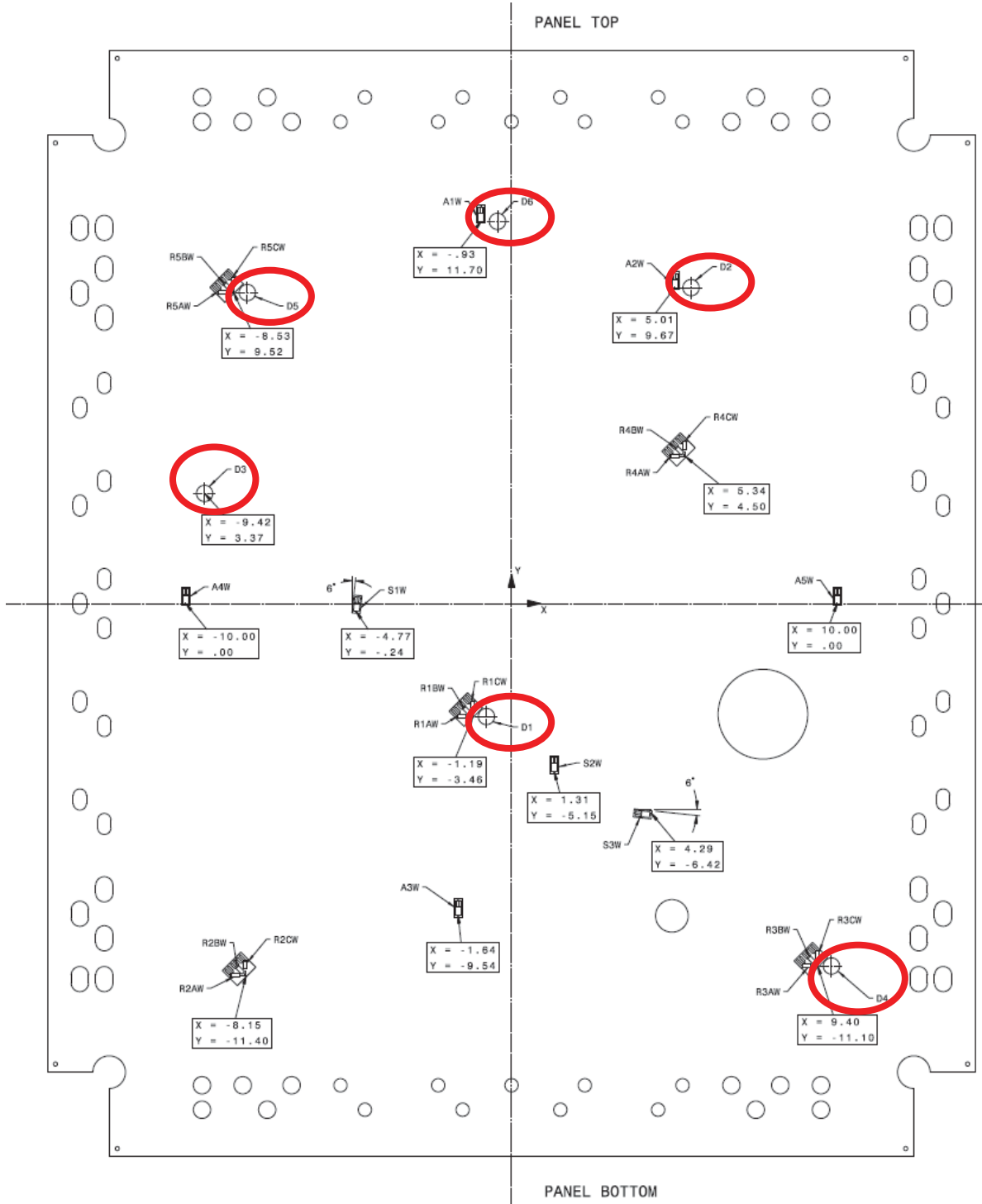


Figure 24. LVDT Locations on Flat Side of Panel.

The out-of-plane displacement predictions did not match the test results. However, this poor correlation is not surprising due to the fabrication issues discussed in Section 5.0. A cross section through the center of the panel is shown below in Figure 25. The neutral axis for this section is approximately 0.08 inch toward the stiffener side of the compression load line causing an induced moment that would cause the test panel to deflect to the stiffener side of the panel (a positive LVDT reading). This is the configuration modeled in the FEM and used for out-of-plane displacement predictions. Unfortunately, the top and bottom of the panel were warped 0.1 inch toward the stiffener side of the panel, effectively shifting the neutral axis at the center of the panel to be located 0.02 inch toward the web side of the applied compression load line. This neutral axis shift will cause the panel to deflect towards the web (flat) side of the panel (a negative LVDT reading).

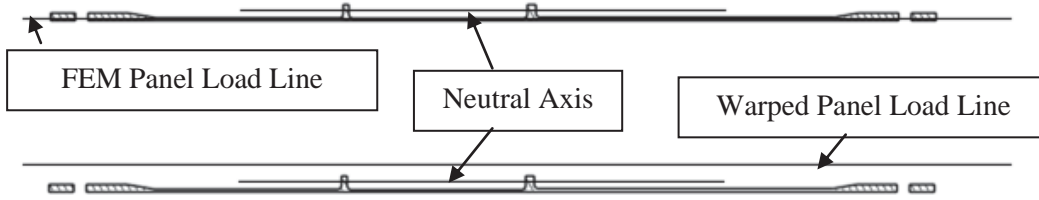


Figure 25. Panel Center Cross Section w/ Neutral Axis Shift.

The shift in the neutral axis due to panel warpage can be seen in the test results shown in Figure 26 for LVDT D1 at the center of the panel. The predicted behavior for deflection to the stiffener side is represented in the positive displacement values. The actual behavior showing deflection to the flat side is represented in the negative LVDT displacement values.

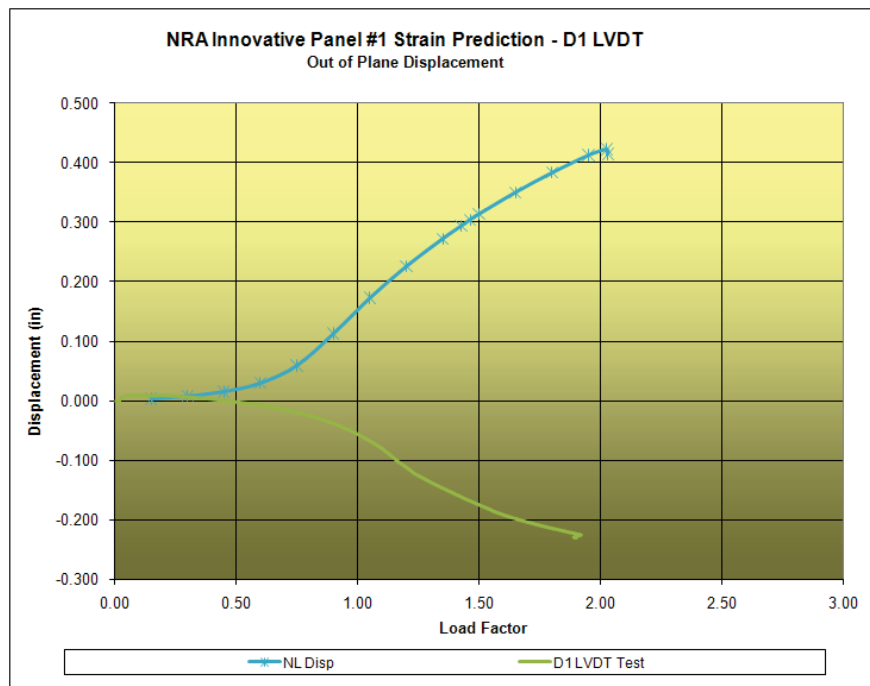


Figure 26. Test Panel Center Out-of Plane-Displacement.

Although a “warped” FEM could be generated and used for predictions, it was decided that such an exercise would only serve to correlate the strain levels for the one-of-a-kind FEM and would not accomplish any further validation of *EBF3PanelOpt*’s buckling optimization capability. The effect of this 0.1-inch out-of-plane warpage in this panel was not included in the panel analysis in this present study.

Additionally, the LVDT’s were located using the results from positive shear predictions. The intent was to place them at peak deflection points for the predicted buckled shape. Because the test was actually performed using an applied negative shear, the locations of the LVDT’s may not be as meaningful as they are no longer located at their intended position on the buckled web. Appendix C contains the data for all 6 LVDT locations (D1-D6).

Strain Predictions

A total of 20 strain gages were attached in back-to-back fashion to the skin of the panel. Ten of the gages were type CEA13-250UR-350 rosettes (0°/45°/90°) rosettes with the 90° direction oriented parallel to the compression load direction. For the strain gage rosettes, the minimum principal strain was calculated from the 0°, 90° and 45° components. Ten of the gages were type CEA00-250UW-350 uniaxial gages oriented parallel to the compression load direction. In addition, 6 more uniaxial gages were attached to the selected stiffeners. Three of these gages were attached to the stiffener and three to the skin directly behind the stiffener on the flat side of the panel. These gages were aligned in the direction of the stiffener. The primary function of the strain gages are to capture the onset of buckling which is why all of the gages are installed “back to back”. The secondary functions of the strain gages are to record the strain levels in each of the panel for test monitoring and comparison to predictions. However, because this panel is sized by buckling and not strength, correlation to magnitude is not critical so long as the test results show buckling to occur as predicted.

Although the onset of buckling, as previously discussed, match the test results very well, the magnitudes for the strain predictions did not match the test results well. This is not surprising due to the fabrication issues discussed in Section 5.0 and the shift in neutral axis (discussed in out of plane displacement results) which caused a change in direction for the induced moment. Moments due to small out of plane displacement (that do not change the overall stiffness of the panel) will affect the strain readings at the outer fibers in the compression direction (vertical rosette leg component), however, will not affect the critical buckling load or the buckling results. The FEM predicted an out of plane deflection towards the stiffener side of the panel. The induced tension should lower the compressive strains on the stiffener side of the panel and increase them on the flat side of the panel. The warped test panel, however, deflected towards the flat side of the panel inducing tension (or a reduction in compression) on the flat side of the panel and adding to the compression of the stiffener side of the panel. Figure 27 shows the predicted strains and test strains.

The results of the predicted behavior versus the test behavior can be seen in this figure. The predicted behavior has lower compressive strains on the stiffener side (R1S) and higher compressive strains on the flat (or web) side (R1W). This behavior is consistent with the prediction assuming out of plane deflection towards the stiffener side. The actual behavior shows lower compressive strains on the flat (or web) side (R1W Min Prin) and higher compressive strains on the stiffener side (R1S Min Prin). This behavior is consistent with a reversal in induced moment caused by the warpage in the panel.

The predicted eigenvalue (0.93) from *EBF3PanelOpt* shown in Figure 27 (blue vertical line) matches well with the onset of buckling seen in the test data (green and orange curves). This match is a

strong indication that the moment reversal caused by the panel warping will change the strain readings, but is not of sufficient magnitude to have an effect on the buckling load level (which is in line with the equations that govern the critical buckling load which are not influenced by moment). The strains from the non-linear FEM run (blue and purple curves) indicated a higher predicted loading as depicted in the higher negative strain readings occurring at a lower percent of limit load. It is not apparent why the non-linear analysis produced this higher local loading; however, it did predict the onset of buckling to occur at the same strain level as the linear analysis. Appendix C contains the data for all of the strain gages.

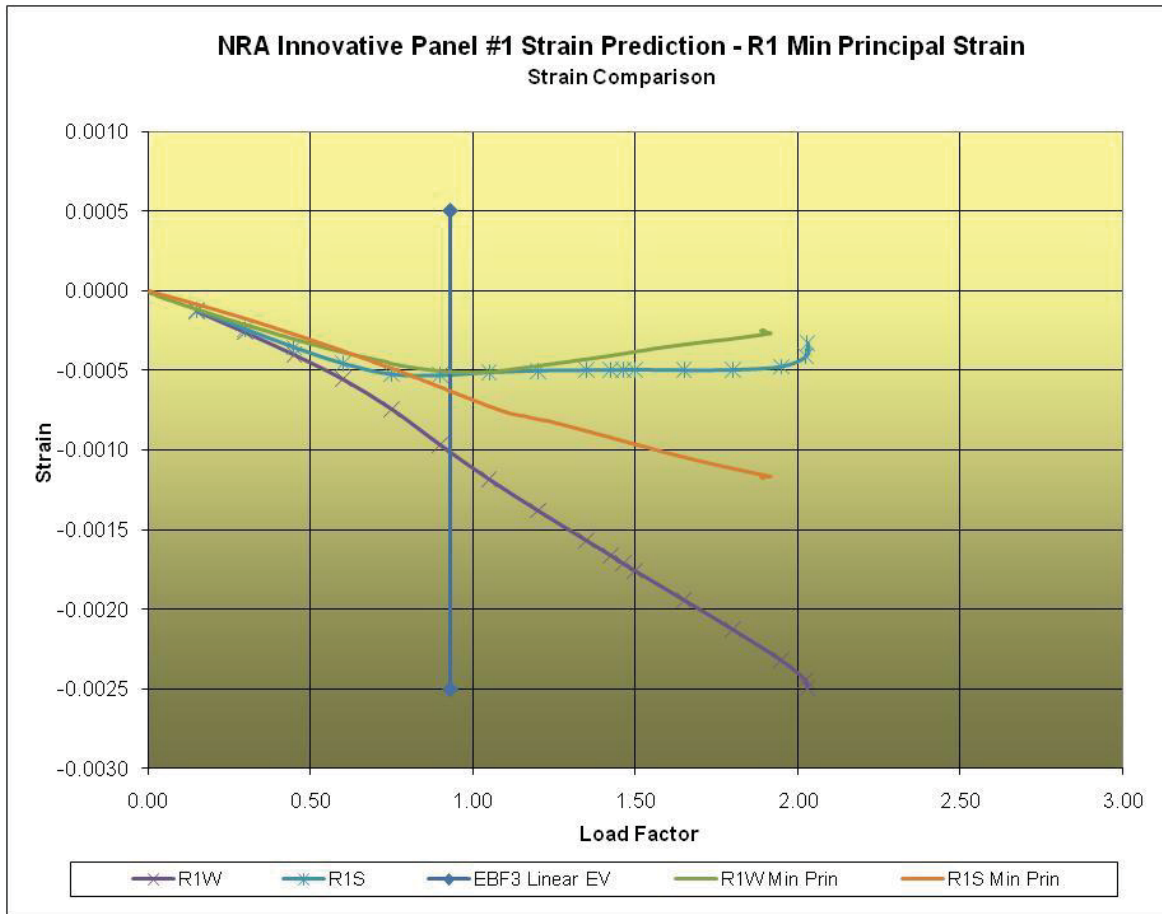


Figure 27. EBF3PanelOpt First Mode Buckling Prediction, Strain Predictions and Test Results. (Strain is presented in inch/inch.)

Figure 28 shows the strain readings from strain gage R2 in the lower right corner of the panel. Yield failure of the material initiated in this corner of the panel, as indicated by the strain reading at a load factor of 2.48 times the analytically derived limit load. This failure load correlated well with the analytical prediction of that occurrence at a load factor of 2.60 times limit load in the same location. A load cell bolt failure ended testing at a load factor of 2.65. The load factor (X-axis) for this figure extends further then the other data shown in this report (and appendix C). All of the data contained in this report and in appendix C reflect the first test that was halted prematurely (load factor of 1.9) due to the shear load cell controller issue discussed previously in Section 6. Once the anomaly in the shear controller was corrected, a second test was performed. Unfortunately, the panel was plastically deformed

during the first test which altered some of the subsequent strain readings during the second test. Although the second test strain readings cannot be compared to prediction, we were able to take the panel to failure to compare location and load level to our predictions.

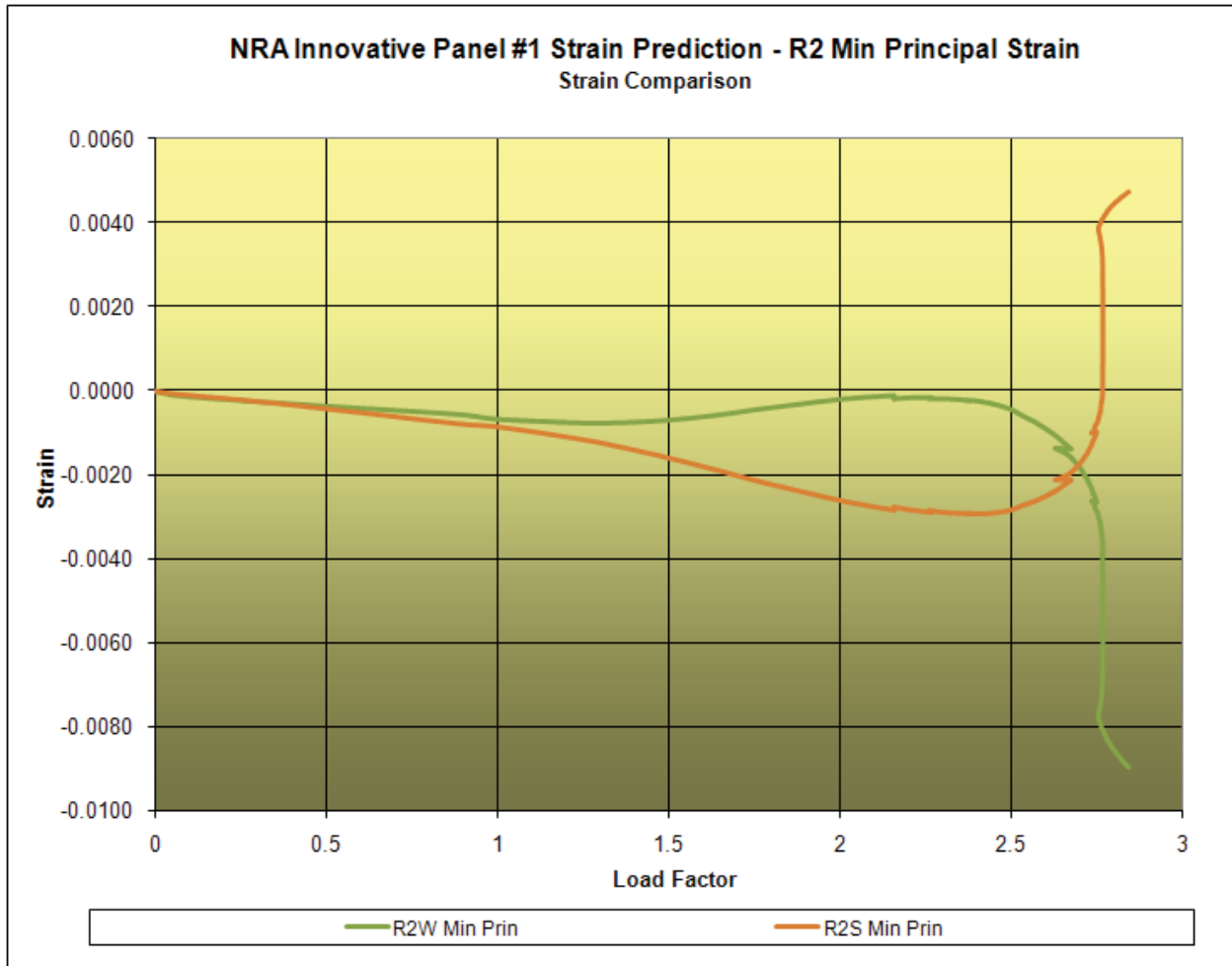


Figure 28. Strain Gage R2 Test Data to Failure. (Strain is presented in inch/inch.)

8 Summary and Conclusions

A new analysis tool, *EBF3PanelOpt*, has been developed for design and optimization of complex multifunctional aircraft structural concepts. The tool was used to design and optimize a structural panel with curved stiffeners. The panel was optimized for minimum mass subjected to combined in-plane loads with constraints on buckling load, yielding, and crippling or local stiffener failure. The resulting design was a panel with a weight of 6.820 lbf, which was about 7% less than the weight of the Lockheed Martin baseline panel with straight stiffeners. The optimized panel design was used to fabricate an integrally-machined test panel using aluminum alloy 2139-T8. The panel was tested under a combined compression-shear loading configuration that is a realistic load case for a large wing pylon rib panel. The test results were compared against analytical results obtained using MSC Nastran. Both a linear FEA which was generated by *EBF3PanelOpt* and a detailed nonlinear FEA were compared with the test results in an attempt to verify the accuracy of assumptions and modeling techniques utilized by the *EBF3PanelOpt* software.

From the comparison of the numerical test results and the finite element analysis the following observations were made:

- Test results show that the panel failed by buckling as predicted by the sizing mode and the buckling occurred at a load close to that predicted by *EBF3PanelOpt*.
- Material yielding begins to occur in the lower corner at a load factor of 2.48, closely matching the predicted behavior and load. Loading continued to a load factor of 2.65 when a load cell bolt failure occurred, ending the testing.
- The strain and deflection predictions, especially in the post buckled region, do not match well to the test results due to the severe warping in the panel. The warp was large enough to shift the neutral axis of the panel to the opposite side of the applied load resulting in a reversal in direction of both out of plane deflection and moment (induced from the eccentricity).

It should be noted that it is not surprising that the post-buckling response is not predicted well by the analysis. The post-buckling response depends heavily on synergistic effects of modeling inaccuracies. Within the nonlinear finite element model, springs are used to introduce the load into the panel. The stiffness of these springs have been tuned and correlated to previous test data.

The accuracy of the predicted response before buckling is a substantial accomplishment and indicates that the information utilized by *EBF3PanelOpt* to predict the buckling, von Mises and crippling constraints are accurate.

Furthermore, this study has shown that it is critical to allow the user to correctly apply the loading and boundary conditions when using *EBF3PanelOpt*. *EBF3PanelOpt* currently allows for uniform loading and uniform clamped, simple or free edge boundary conditions.

References

1. Baker, D.J., "Combined Load Test Fixture," Technical Memorandum ARL-TR-3726, Army Research Lab, Hampton, VA, February 2006.
2. Gurav, S. P. and Kapania, R. K., "Development of Framework for the Design Optimization of Unitized Structures," 50th AIAA/ASME/ASCE/AHS/ASC Structures, Structural Dynamics, and Materials Conference, Palm Springs, CA, May 4-7, 2009, AIAA2009-2186.
3. Joshi, P., Mulani, S. B., Kapania, R. K. and Shin, Y. S., "Optimal Design of Unitized Structures with Curvilinear Stiffeners Using Response Surface Methodology", AIAA-2008-2304, 49th AIAA/ASME/ASCE/AHS/ASC Structures, Structural Dynamics, and Materials Conference 16th AIAA/ASME/AHS Adaptive Structures Conference, Schaumburg, IL, Apr. 7-10, 2008.
4. Joshi, P., Mulani, S. B., Gurav, S. P., and Kapania, R. K., "Design Optimization for Minimum Sound Radiation from Point-Excited Curvilinearly Stiffened Panel", 50th AIAA/ASME/ASCE/AHS/ASC Structures, Structural Dynamics, and Materials Conference 17th AIAA/ASME/AHS Adaptive Structures Conference, Palm Springs, California, May 4-7, 2009, AIAA-2009-2649.
5. Dang, T. D., Kapania, R. K. and Gurav, S. P., "Optimization of Unitized Structures under Damage Tolerance Constraints," 50th AIAA/ASME/ASCE/AHS/ASC Structures, Structural Dynamics, and Materials Conference 17th AIAA/ASME/AHS Adaptive Structures Conference, Palm Springs, California, May 4-7, 2009, AIAA-2009-2550.
6. Niu, M.C.Y., ed. Airframe Stress Analysis and Sizing. 2nd. Hong Cong: Conmilit Press, 1997
7. Venter, G. and Sobieszczanski-Sobieski, J. "Particle Swarm Optimization," 43rd AIAA/ASME/ASCE/AHS/ASC Structures, Structural Dynamics, and Materials Conference, Denver, CO, April 22-25, 2002, AIAA2002-1235.

Appendix A

Strain Gage Locations

A total of 20 strain gages were attached in back-to-back fashion to the skin of the panel. Ten of the gages were type CEA13-250UR-350 rosettes ($0^\circ/45^\circ/90^\circ$) with the 90° direction oriented parallel to the compression load direction. Ten of the gages were type CEA00-250UW-350 uniaxial gages oriented parallel to the compression load direction. Six additional uniaxial gages were attached to the selected stiffeners. Three of these gages were attached to the stiffener and three to the skin directly behind the stiffener on the flat side of the panel. These gages were aligned in the direction of the stiffener.

Table A1 shows an itemized list of the strain gages and their location on the panel. Figure A1 shows the strain gage locations on the stiffener side of the panel. The corresponding gages for the flat side of the panel are directly behind those shown in the figure. The intersection of the vertical and horizontal centerlines is considered to be the zero position point on the panel. When viewing the stiffened side of the panel, the positive horizontal direction (x) is moving to the right. The positive vertical direction (y) is moving upward. The bottom stiffener is Stiffener A and the top stiffener is Stiffener D. The left-hand stiffener is Stiffener B and the right-hand stiffener is Stiffener C. The strain gage locations for Stiffeners A, B, and C are shown in figures A2, A3, and A4, respectively.

Table A1. Location of Strain Gages on Compression-Shear Test Panel.

| gage ID | gage type | orient. | x (in.) | y (in.) | location | Figure |
|---------|-----------|---------|---------|---------|---|--------|
| A1S | uniaxial | 90° | 0.93 | 11.70 | Skin on stiffener side of panel | A1 |
| A1W | uniaxial | 90° | 0.93 | 11.70 | Skin on flat side of panel | |
| A2S | uniaxial | 90° | -5.01 | 9.67 | Skin on stiffener side of panel | A1 |
| A2W | uniaxial | 90° | -5.01 | 9.67 | Skin on flat side of panel | |
| A3S | uniaxial | 90° | 1.64 | -9.54 | Skin on stiffener side of panel | A1 |
| A3W | uniaxial | 90° | 1.64 | -9.54 | Skin on flat side of panel | |
| A4S | uniaxial | 90° | 10.00 | 0.00 | Skin on stiffener side of panel | A1 |
| A4W | uniaxial | 90° | 10.00 | 0.00 | Skin on flat side of panel | |
| A5S | uniaxial | 90° | -10.00 | 0.00 | Skin on stiffener side of panel | A1 |
| A5W | uniaxial | 90° | -10.00 | 0.00 | Skin on flat side of panel | |
| R1AS | rosette | 0° | 1.19 | -3.46 | Skin on stiffener side of panel | A1 |
| R1BS | rosette | 45° | 1.19 | -3.46 | Skin on stiffener side of panel | A1 |
| R1CS | rosette | 90° | 1.19 | -3.46 | Skin on stiffener side of panel | A1 |
| R1AW | rosette | 0° | 1.19 | -3.46 | Skin on flat side of panel | |
| R1BW | rosette | 45° | 1.19 | -3.46 | Skin on flat side of panel | |
| R1CW | rosette | 90° | 1.19 | -3.46 | Skin on flat side of panel | |
| R2AS | rosette | 0° | 8.15 | -11.40 | Skin on stiffener side of panel | A1 |
| R2BS | rosette | 45° | 8.15 | -11.40 | Skin on stiffener side of panel | A1 |
| R2CS | rosette | 90° | 8.15 | -11.40 | Skin on stiffener side of panel | A1 |
| R2AW | rosette | 0° | 8.15 | -11.40 | Skin on flat side of panel | |
| R2BW | rosette | 45° | 8.15 | -11.40 | Skin on flat side of panel | |
| R2CW | rosette | 90° | 8.15 | -11.40 | Skin on flat side of panel | |
| R3AS | rosette | 0° | -9.40 | -11.10 | Skin on stiffener side of panel | A1 |
| R3BS | rosette | 45° | -9.40 | -11.10 | Skin on stiffener side of panel | A1 |
| R3CS | rosette | 90° | -9.40 | -11.10 | Skin on stiffener side of panel | A1 |
| R3AW | rosette | 0° | -9.40 | -11.10 | Skin on flat side of panel | |
| R3BW | rosette | 45° | -9.40 | -11.10 | Skin on flat side of panel | |
| R3CW | rosette | 90° | -9.40 | -11.10 | Skin on flat side of panel | |
| R4AS | rosette | 0° | -5.34 | 4.50 | Skin on stiffener side of panel | A1 |
| R4BS | rosette | 45° | -5.34 | 4.50 | Skin on stiffener side of panel | A1 |
| R4CS | rosette | 90° | -5.34 | 4.50 | Skin on stiffener side of panel | A1 |
| R4AW | rosette | 0° | -5.34 | 4.50 | Skin on flat side of panel | |
| R4BW | rosette | 45° | -5.34 | 4.50 | Skin on flat side of panel | |
| R4CW | rosette | 90° | -5.34 | 4.50 | Skin on flat side of panel | |
| R5AS | rosette | 0° | 8.53 | 9.52 | Skin on stiffener side of panel | A1 |
| R5BS | rosette | 45° | 8.53 | 9.52 | Skin on stiffener side of panel | A1 |
| R5CS | rosette | 90° | 8.53 | 9.52 | Skin on stiffener side of panel | A1 |
| R5AW | rosette | 0° | 8.53 | 9.52 | Skin on flat side of panel | |
| R5BW | rosette | 45° | 8.53 | 9.52 | Skin on flat side of panel | |
| R5CW | rosette | 90° | 8.53 | 9.52 | Skin on flat side of panel | |
| S1S | uniaxial | 90° | 4.68 | -0.29 | Stiffener C | A4 |
| S1W | uniaxial | 90° | 4.68 | -0.29 | Skin on flat side of panel behind Stiffener C | |
| S2S | uniaxial | 90° | -1.45 | -5.20 | Stiffener B | A3 |
| S2W | uniaxial | 90° | -1.45 | -5.20 | Skin on flat side of panel behind Stiffener B | |
| S3S | uniaxial | 90° | -4.29 | -6.45 | Stiffener A | A2 |
| S3W | uniaxial | 90° | -4.29 | -6.45 | Skin on flat side of panel behind Stiffener A | |

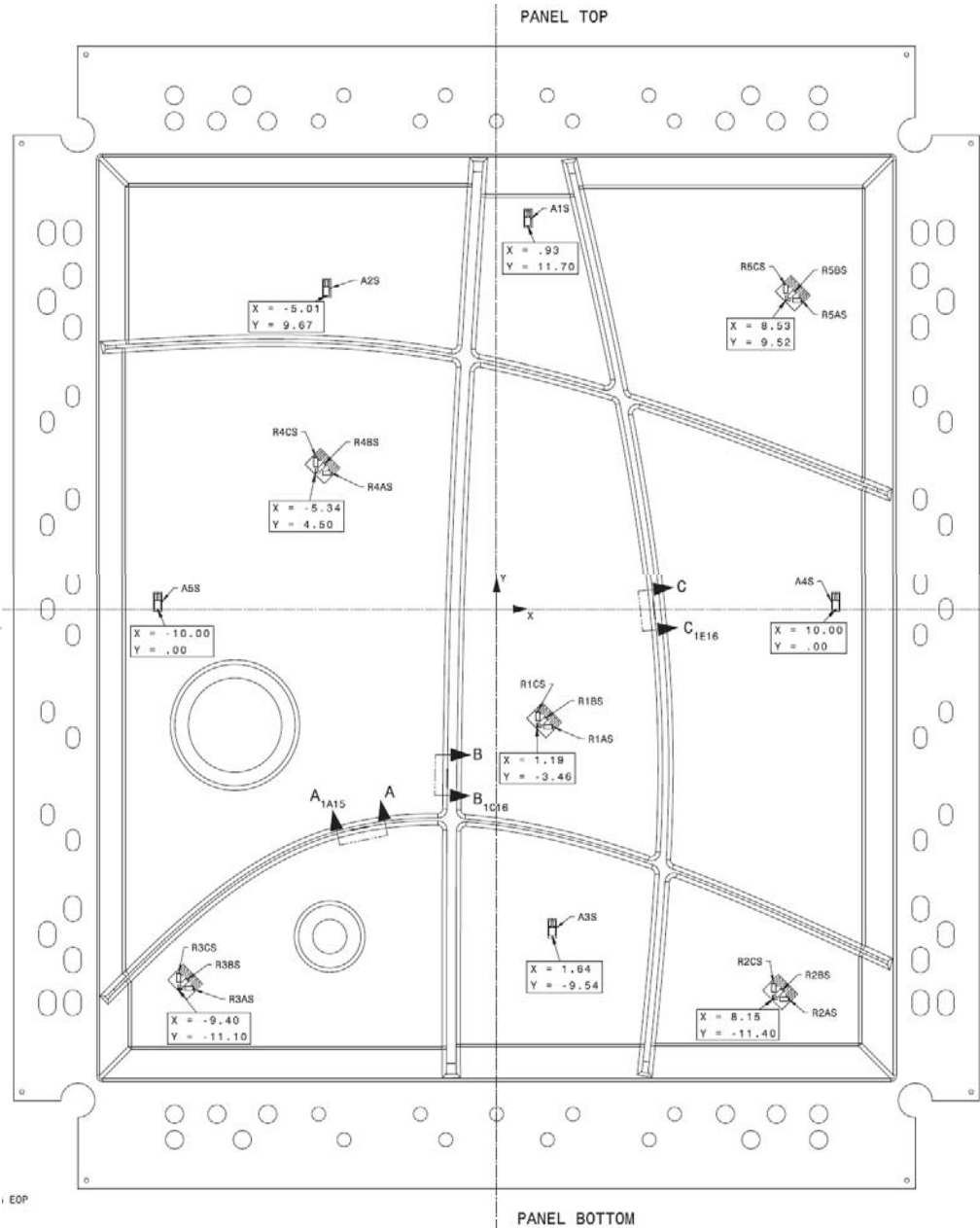


Figure A1. Location of Strain Gages on Stiffener Side of Panel.

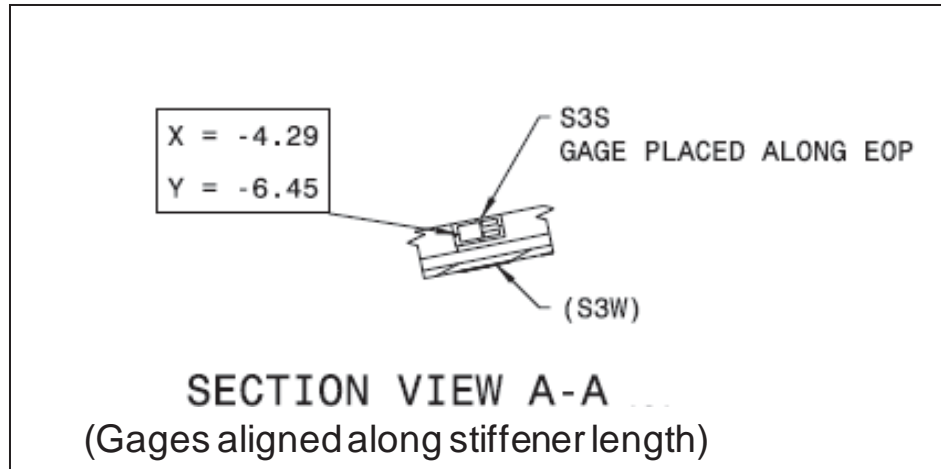


Figure A2. Location of strain gages on Stiffener A.

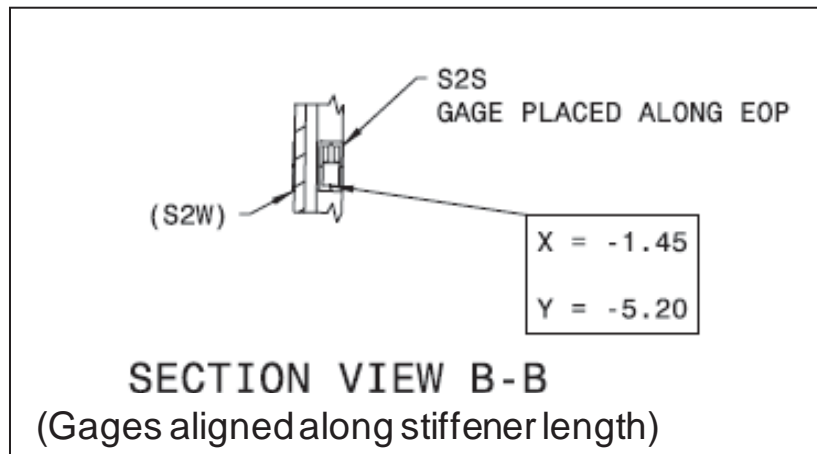


Figure A3. Location of strain gages on Stiffener B.

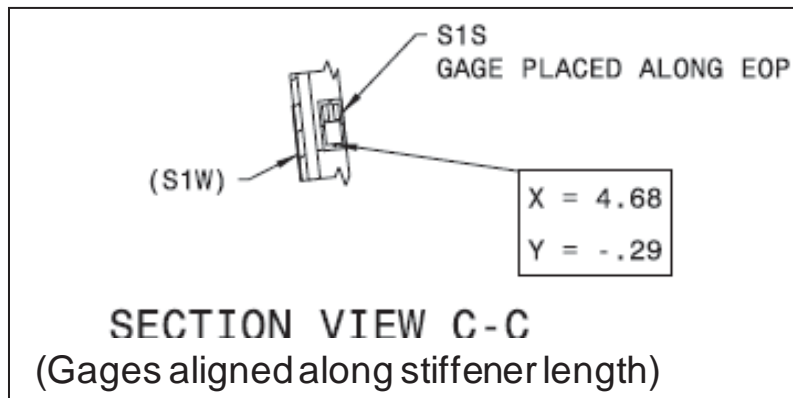


Figure A4. Location of Strain Gages on Stiffener C

Appendix B

Location of LVDTs for Out-of-Plane Displacement Measurement

A total of 6 linear variable displacement transducers (LVDTs) were attached to the compression-shear test panel to measure out-of-plane displacement. The LVDTs were attached to the flat side of the panel using mounting brackets attached to the test machine. The LVDTs were configured such that buckling of the skin towards the stiffener side of the panel would result in a positive displacement reading on the data acquisition system. Table B1 shows an itemized list of the LVDTs and their location on the panel. Figure B1 shows photos of (a) the top half and (b) the bottom half of the flat side of the panel with the LVDTs attached. The intersection of the vertical and horizontal centerlines of the panel is considered to be the zero position point on the panel. When viewing the stiffened side of the panel, the positive horizontal direction (x) is moving to the right. The positive vertical direction (y) is moving upward.

Table B1. Location of LVDTs on Compression-Shear Test Panel.

| LVDT no. | X (in.) | Y (in.) |
|----------|---------|---------|
| D1 | 1.2 | -3.6 |
| D2 | -4.8 | 10.0 |
| D3 | 9.7 | 2.8 |
| D4 | -9.4 | -11.3 |
| D5 | 8.5 | 9.9 |
| D6 | 0.8 | 12.2 |

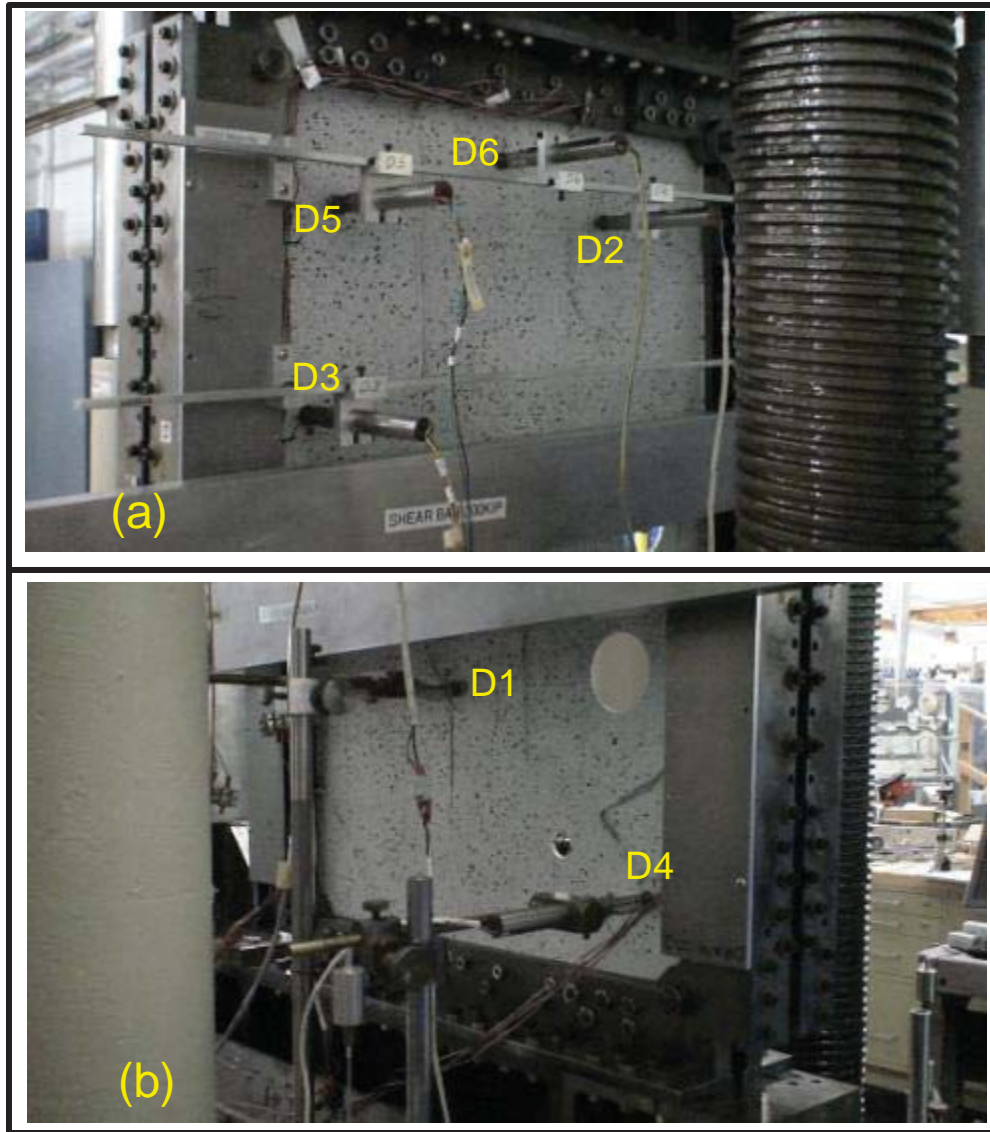


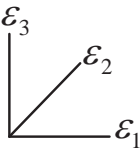
Figure B1. Location of LVDTs on Flat Side of Test Panel for Out-of-Plane Displacement Measurement: (a) Top Half of Panel; (b) Bottom Half of Panel.

Appendix C

Supplemental Data from Strain Gages and the Out-of-Plane LDVTs

The results from each LDVT and strain gage are plotted in figures C1-C17. For the strain gage rosettes, the minimum principal strain was calculated from the 0°, 90° and 45° components using the following equation:

Principal Stresses with
0-45-90° Rosette:



$$\sigma_{MAX/MIN} = \frac{E}{2} \left[\frac{\varepsilon_1 + \varepsilon_3}{1-\nu} \pm \frac{\sqrt{2}}{1+\nu} \sqrt{(\varepsilon_1 - \varepsilon_2)^2 + (\varepsilon_2 - \varepsilon_3)^2} \right]$$

The minimum principal strain predictions from the nonlinear finite analysis are also included in the strain plots. For the LVDT data, positive displacement is towards the stiffener side of the panel. Refer to appendix A for strain gage locations and appendix B for out-of-plane LVDT locations.

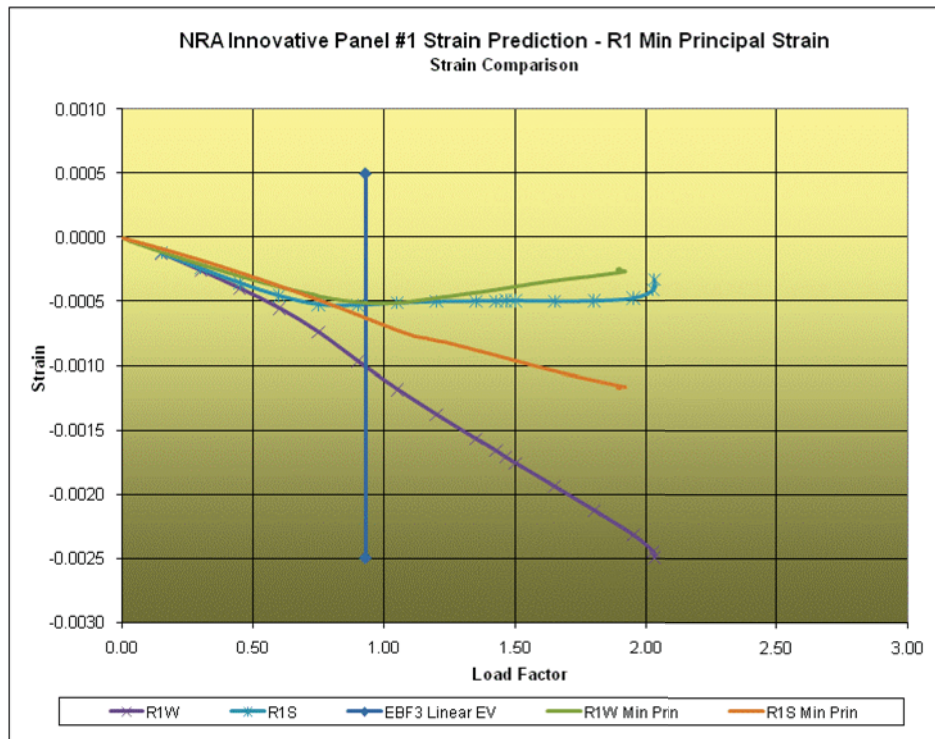


Figure C1. Strain Gage R1 Data. (Strain is presented in inch/inch).

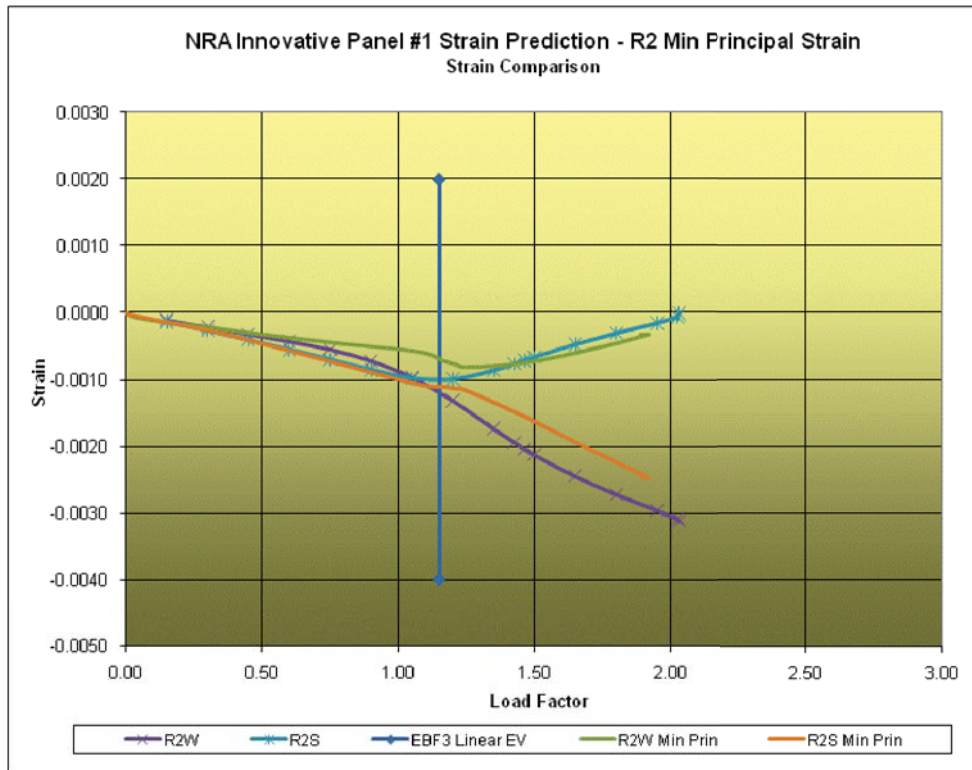


Figure C2. Strain Gage R2 Data. (Strain is presented in inch/inch).

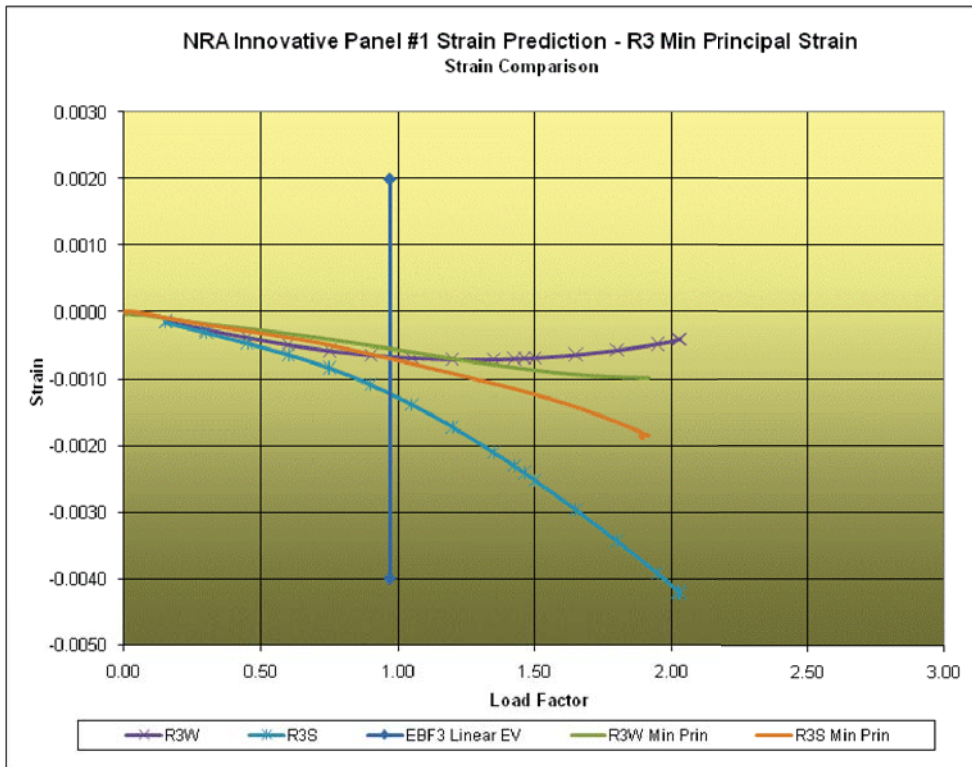


Figure C3. Strain Gage R3 Data. (Strain is presented in inch/inch).

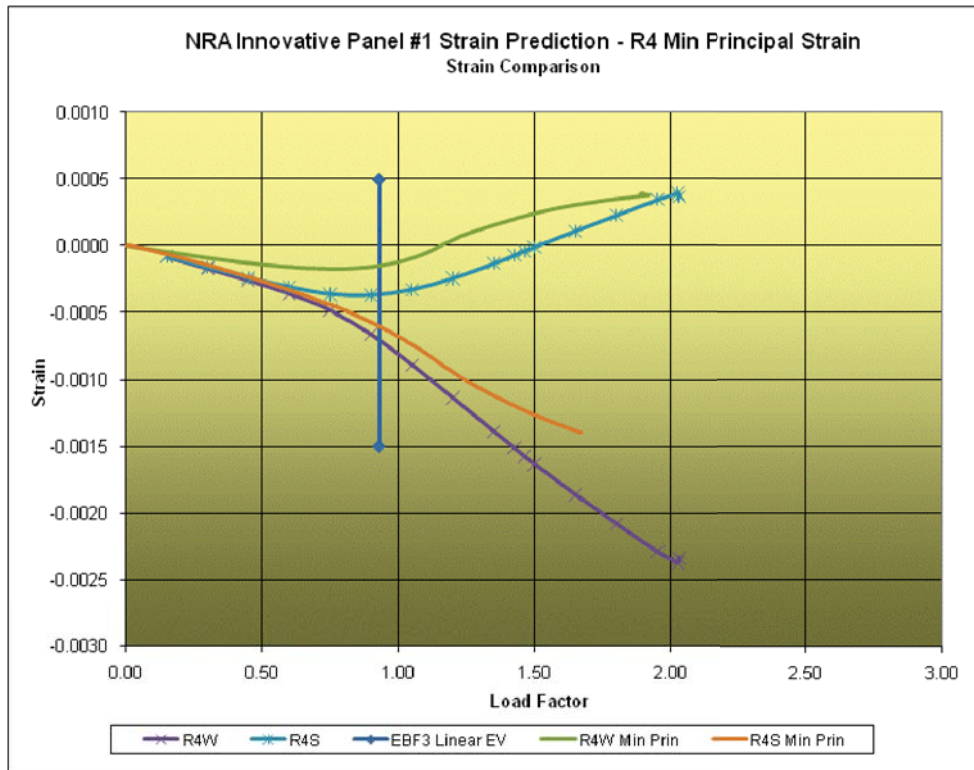


Figure C4. Strain Gage R4 Data. (Strain is presented in inch/inch).

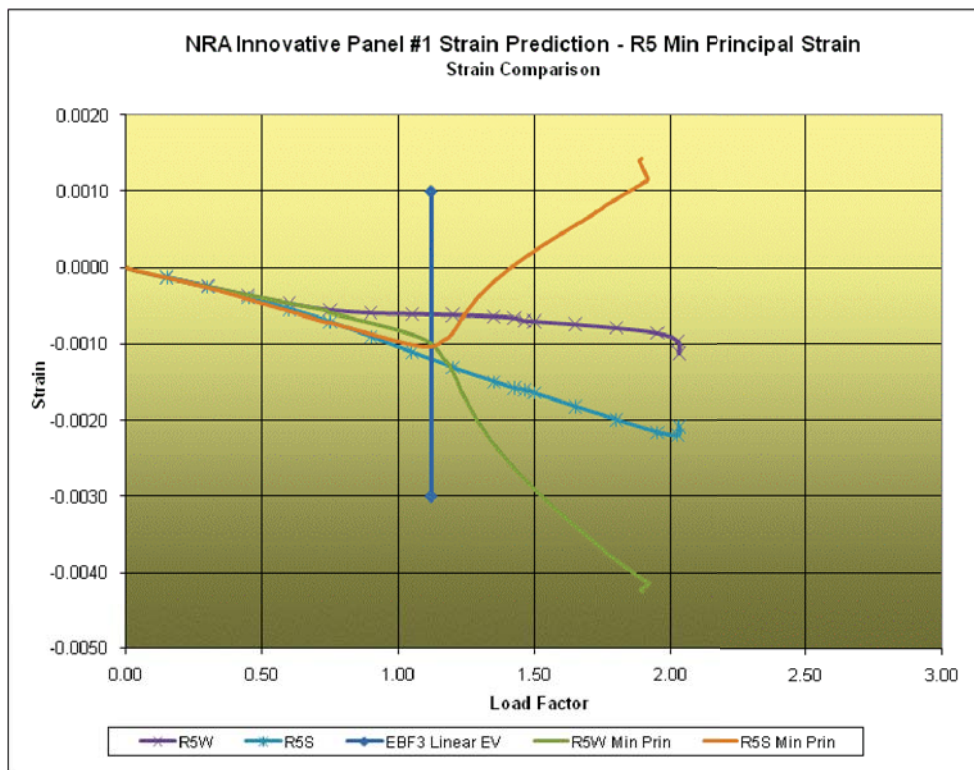


Figure C5. Strain Gage R5 Data. (Strain is presented in inch/inch).

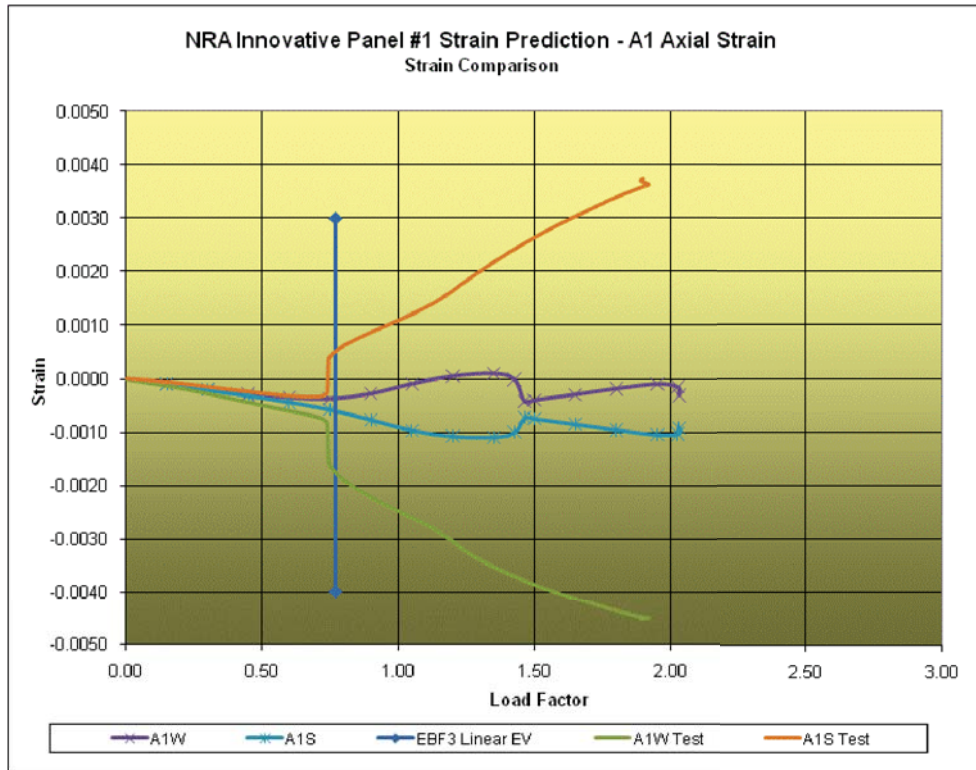


Figure C6. Strain Gage A1 Data. (Strain is presented in inch/inch).

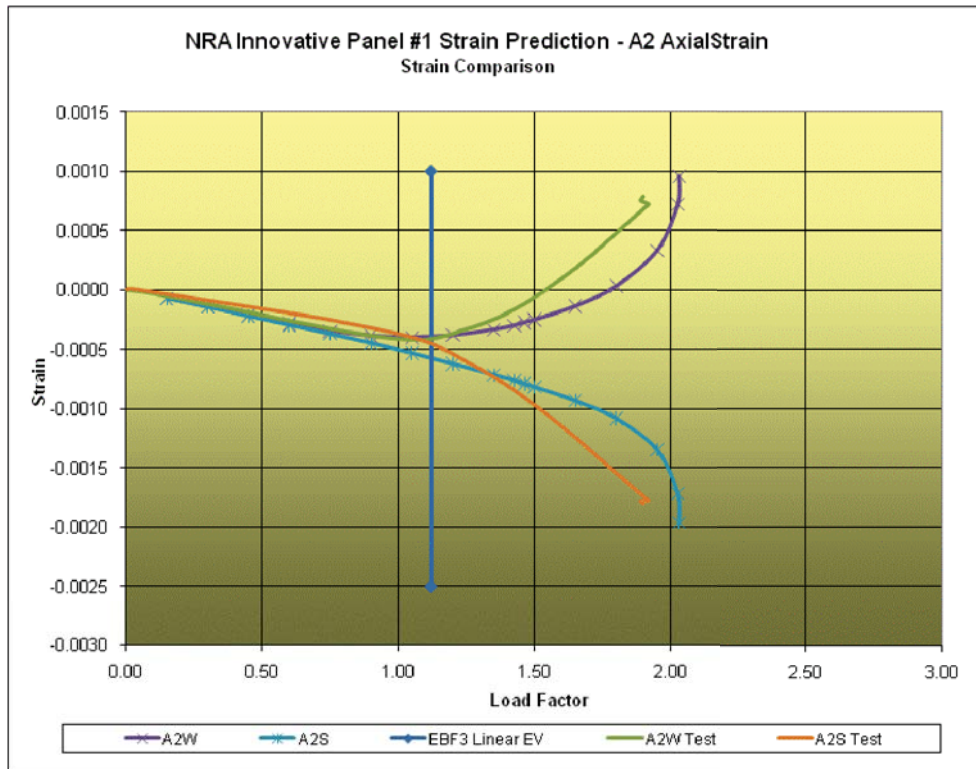


Figure C7. Strain Gage A2 Data. (Strain is presented in inch/inch).

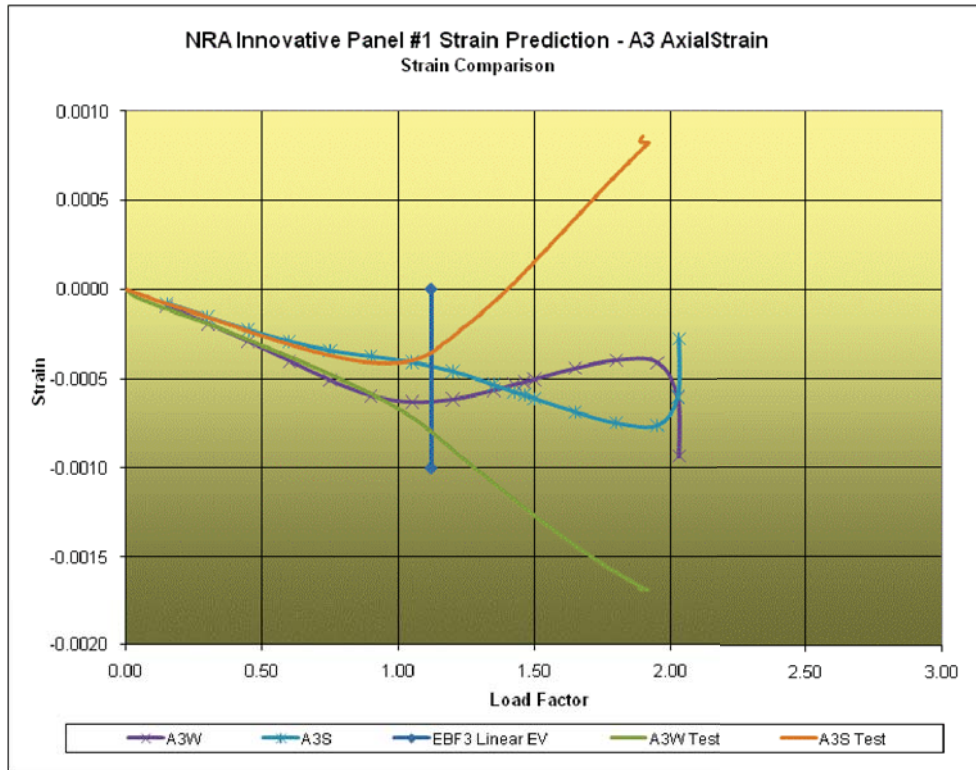


Figure C8. Strain Gage A3 Data. (Strain is presented in inch/inch).

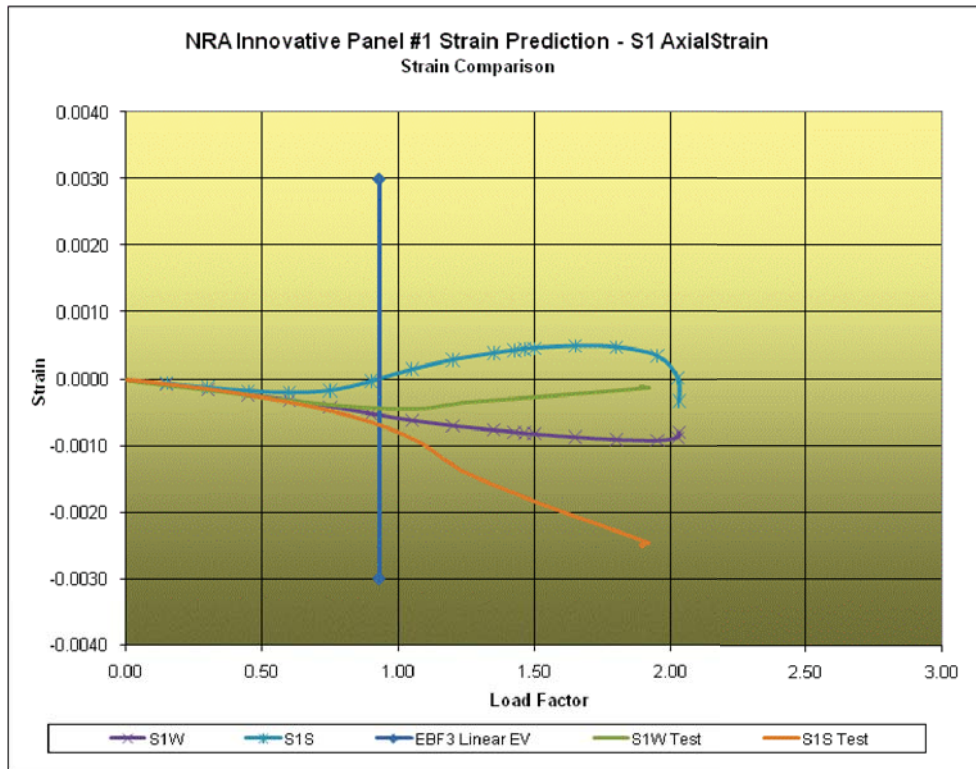


Figure C9. Strain Gage S1 Data. (Strain is presented in inch/inch).

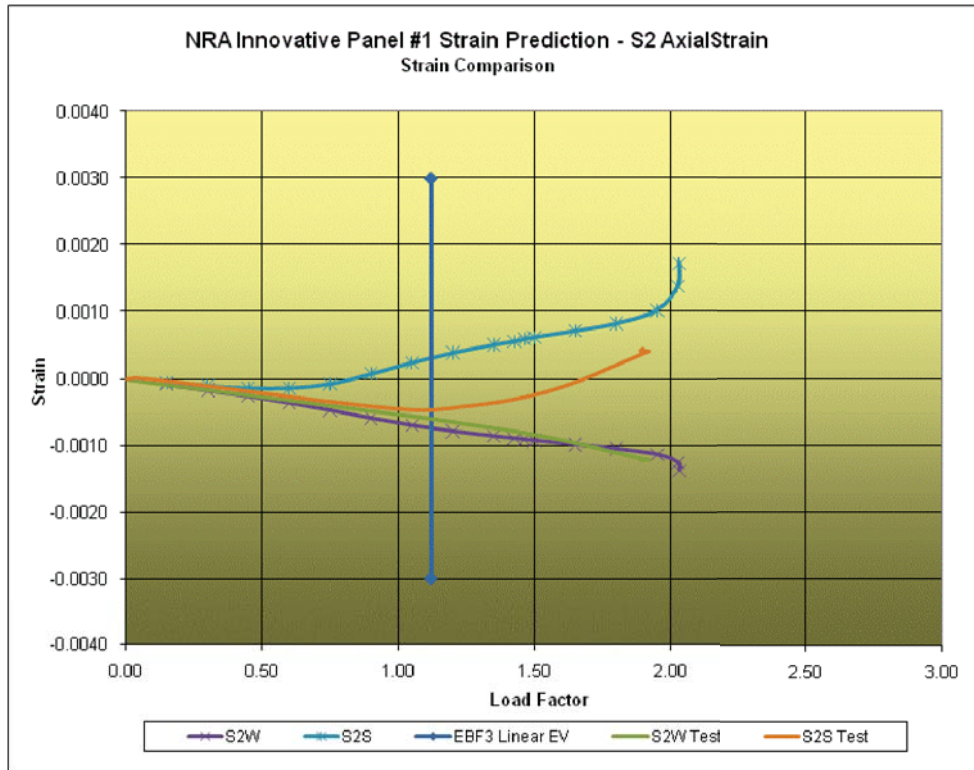


Figure C10. Strain Gage S2 Data. (Strain is presented in inch/inch).

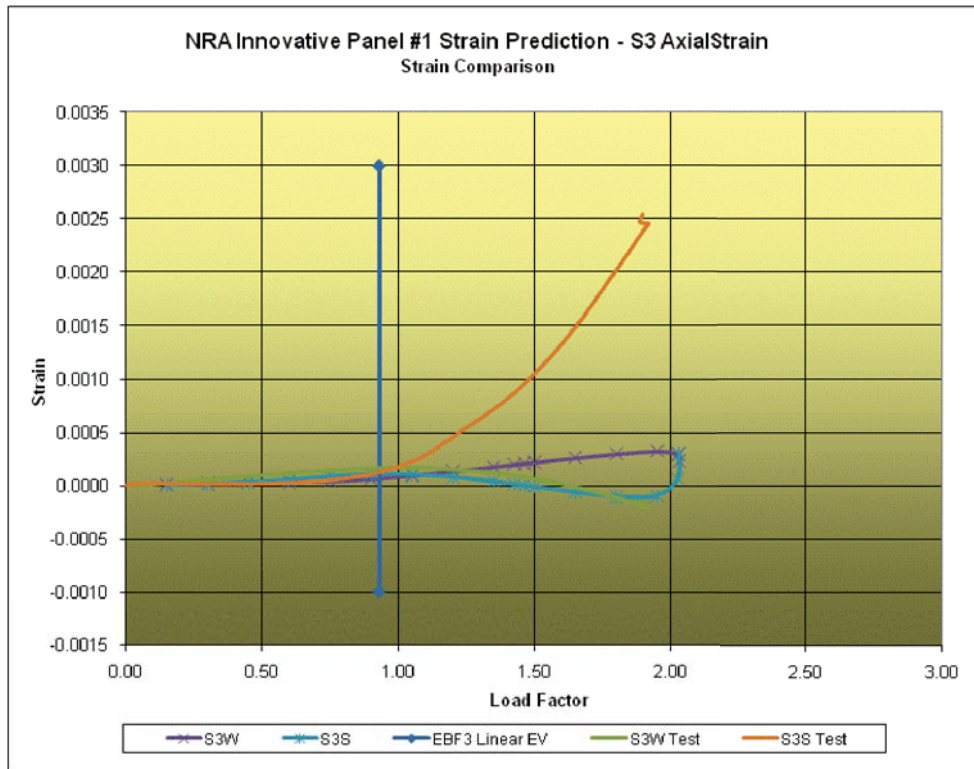


Figure C11. Strain Gage S3 Data. (Strain is presented in inch/inch).

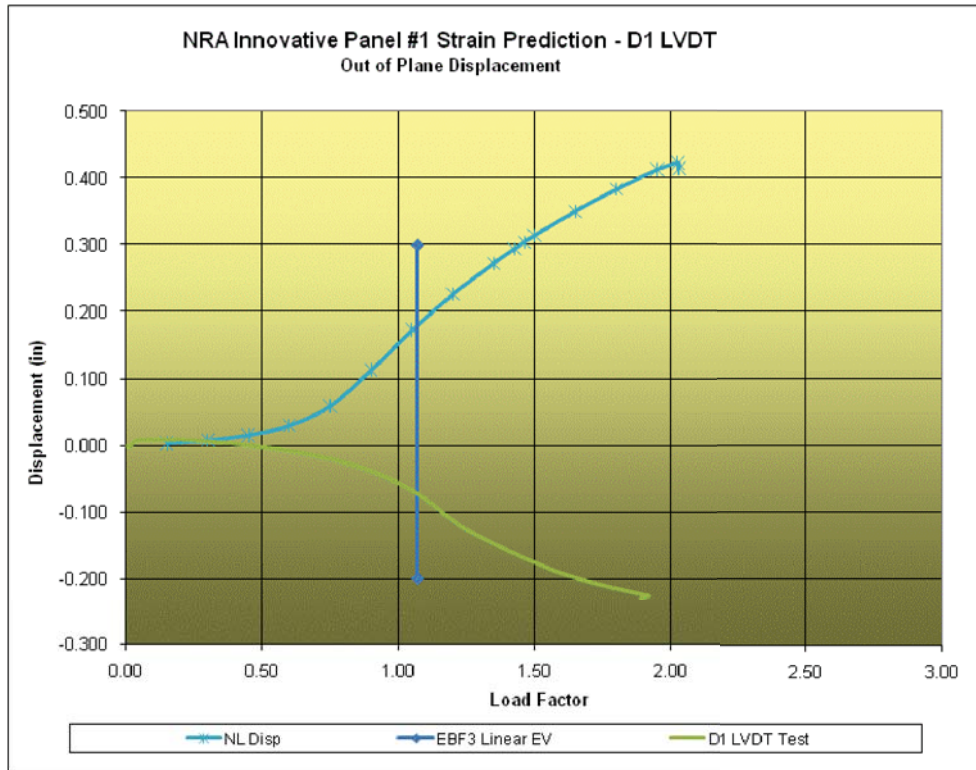


Figure C12. D1 LVDT Data.

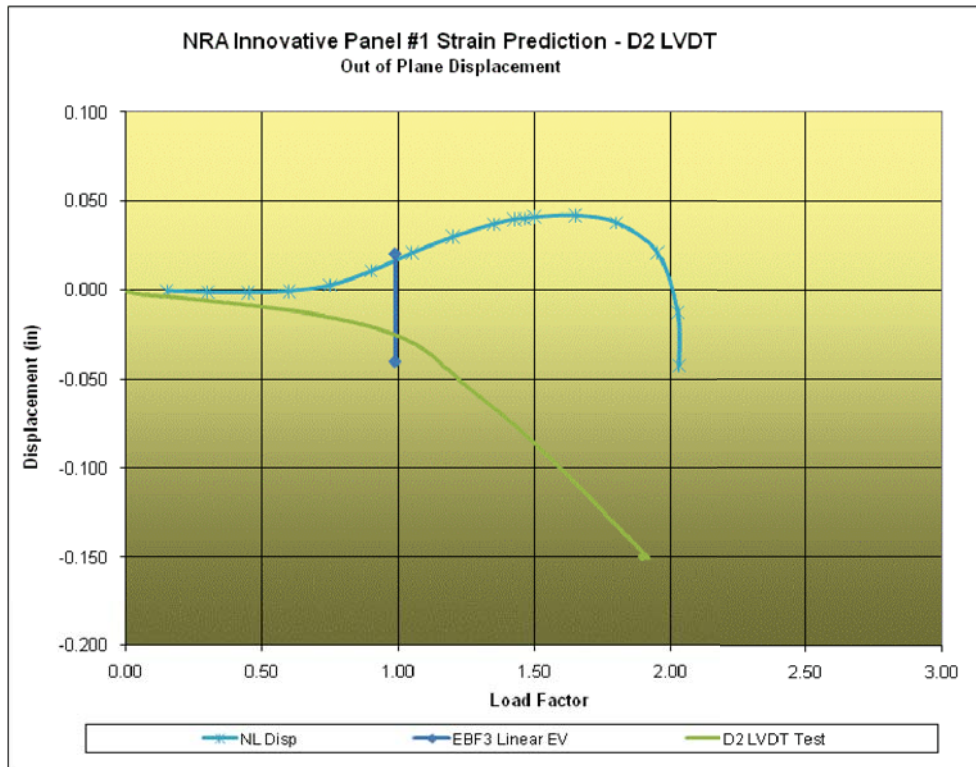


Figure C13. D2 LVDT Data.

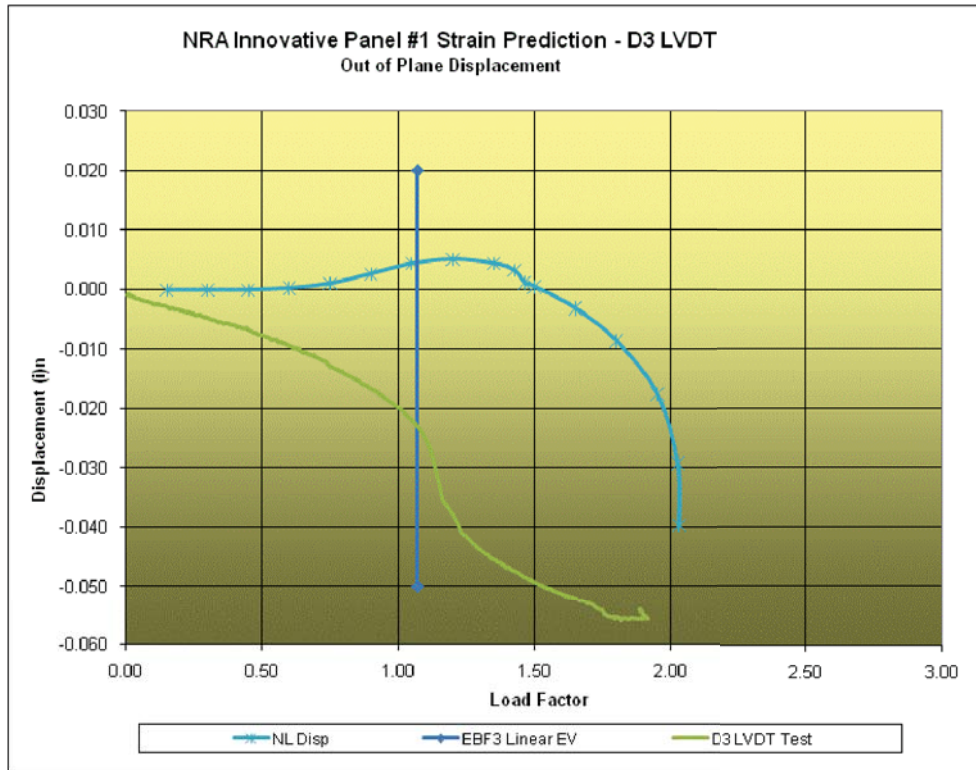


Figure C14. D3 LVDT Data.

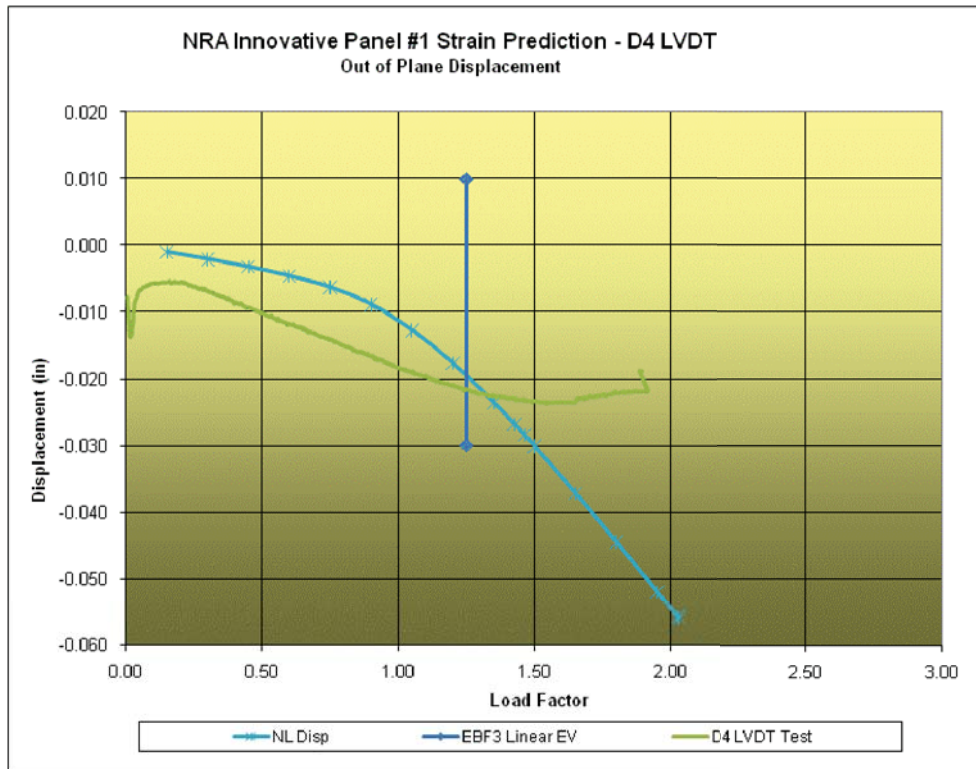


Figure C15. D4 LVDT Data.

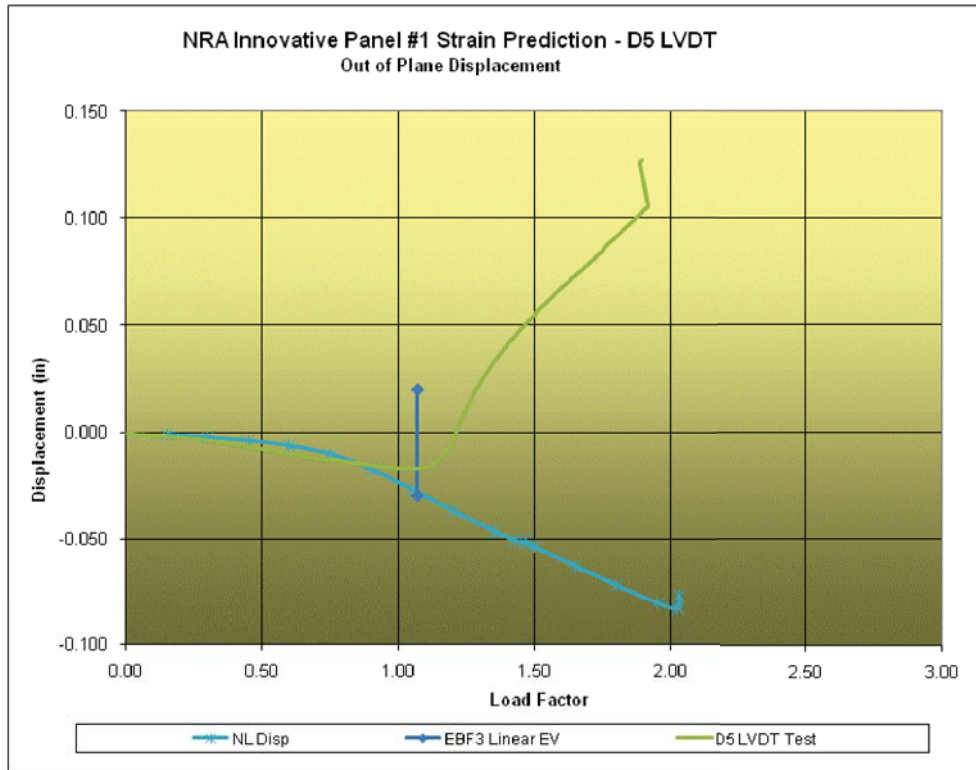


Figure C16. D5 LVDT Data.

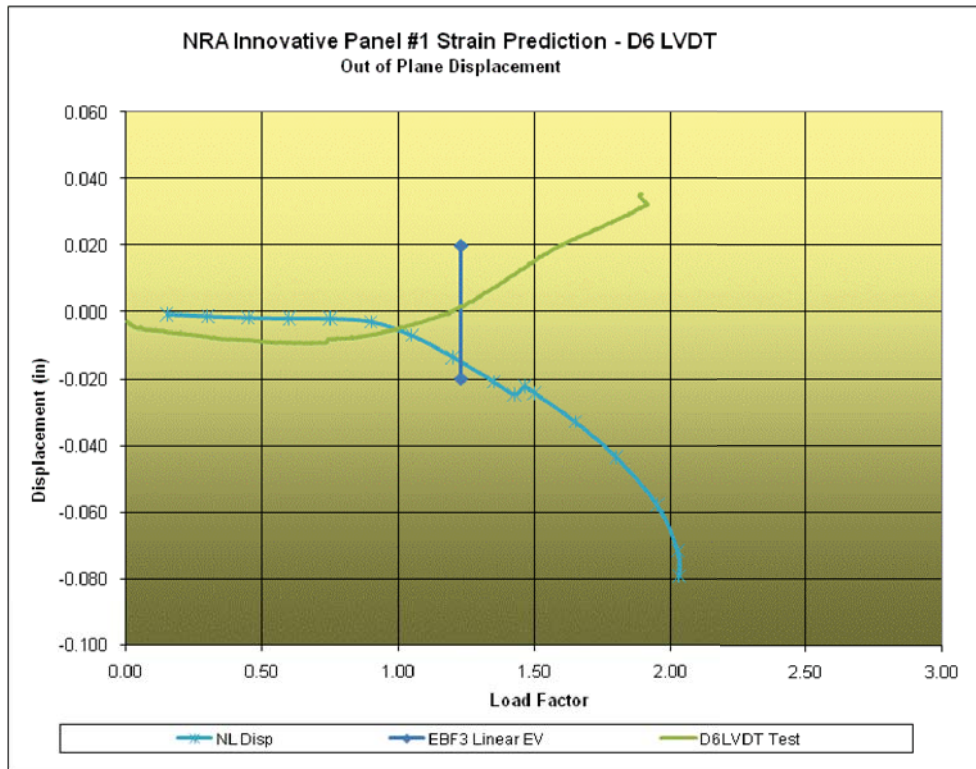


Figure C17. D6 LVDT Data.

| REPORT DOCUMENTATION PAGE | | | Form Approved OMB No. 0704-0188 | | |
|--|-------------|--|---|------------------------------|---|
| <p>The public reporting burden for this collection of information is estimated to average 1 hour per response, including the time for reviewing instructions, searching existing data sources, gathering and maintaining the data needed, and completing and reviewing the collection of information. Send comments regarding this burden estimate or any other aspect of this collection of information, including suggestions for reducing this burden, to Department of Defense, Washington Headquarters Services, Directorate for Information Operations and Reports (0704-0188), 1215 Jefferson Davis Highway, Suite 1204, Arlington, VA 22202-4302. Respondents should be aware that notwithstanding any other provision of law, no person shall be subject to any penalty for failing to comply with a collection of information if it does not display a currently valid OMB control number.</p> <p>PLEASE DO NOT RETURN YOUR FORM TO THE ABOVE ADDRESS.</p> | | | | | |
| 1. REPORT DATE (DD-MM-YYYY) 01-11-2011 | | 2. REPORT TYPE Technical Memorandum | | 3. DATES COVERED (From - To) | |
| 4. TITLE AND SUBTITLE Design, Optimization, and Evaluation of Integrally-Stiffened A1-2139 Panel With Curved Stiffeners | | | 5a. CONTRACT NUMBER | | |
| | | | 5b. GRANT NUMBER | | |
| | | | 5c. PROGRAM ELEMENT NUMBER | | |
| 6. AUTHOR(S) Havens, David; Shiyekar, Sandeep; Norris, Ashley; Bird, Richard K.; Kapania, Rakesh K.; Olliffe, Robert | | | 5d. PROJECT NUMBER | | |
| | | | 5e. TASK NUMBER | | |
| | | | 5f. WORK UNIT NUMBER 561581.02.08.07.15.15 | | |
| 7. PERFORMING ORGANIZATION NAME(S) AND ADDRESS(ES) NASA Langley Research Center Hampton, VA 23681-2199 | | | 8. PERFORMING ORGANIZATION REPORT NUMBER L-20097 | | |
| 9. SPONSORING/MONITORING AGENCY NAME(S) AND ADDRESS(ES) National Aeronautics and Space Administration Washington, DC 20546-0001 | | | 10. SPONSOR/MONITOR'S ACRONYM(S) NASA | | |
| | | | 11. SPONSOR/MONITOR'S REPORT NUMBER(S) NASA/TM-2011-217308 | | |
| 12. DISTRIBUTION/AVAILABILITY STATEMENT Unclassified - Unlimited Subject Category 39 Availability: NASA CASI (443) 757-5802 | | | | | |
| 13. SUPPLEMENTARY NOTES | | | | | |
| 14. ABSTRACT A curvilinear stiffened panel was designed, manufactured, and tested in the Combined Load Test Fixture at NASA Langley Research Center. The panel is representative of a large wing engine pylon rib and was optimized for minimum mass subjected to three combined load cases. The optimization included constraints on web buckling, material yielding, crippling or local stiffener failure, and damage tolerance using a new analysis tool named EBF3PanelOpt. Testing was performed for the critical combined compression-shear loading configuration. The panel was loaded beyond initial buckling, and strains and out-of-plane displacements were extracted from a total of 20 strain gages and 6 linear variable displacement transducers. The VIC-3D system was utilized to obtain full field displacements/strains in the stiffened side of the panel. The experimental data were compared with the strains and out-of-plane deflections from a high fidelity nonlinear finite element analysis. The experimental data were also compared with linear elastic finite element results of the panel/test-fixture assembly. Overall, the panel buckled very near to the predicted load in the web regions. | | | | | |
| 15. SUBJECT TERMS Curvilinear stiffeners; Finite element analysis; Load tests; Structural design; Structural optimization | | | | | |
| 16. SECURITY CLASSIFICATION OF: | | | 17. LIMITATION OF ABSTRACT | 18. NUMBER OF PAGES | 19a. NAME OF RESPONSIBLE PERSON |
| a. REPORT | b. ABSTRACT | c. THIS PAGE | | | STI Help Desk (email: help@sti.nasa.gov) |
| U | U | U | UU | 48 | 19b. TELEPHONE NUMBER (Include area code) (443) 757-5802 |